4. DATA ACQUISITION

Samples were collected from the Tailings Storage Facility on 7 and 8 July 2011 as well as 20 February 2012. The tailings material was subsequently analysed to provide an understanding of the chemical composition and -behaviour in order to model the liberation of potential contaminants. The material, as well as the underlying aquifer, was also hydraulically tested to provide an understanding of the hydraulic properties to obtain flow and contaminant transport properties. This was also helpful in determining hydraulic boundary conditions.

4.1 Sampling Methods

4.1.1 Hand Auger Drilling

Hand auger drilling was employed to sample the tailings material in 2011. This method was chosen as it is cost effective, the tailings material is readily removed via this method and it provides a generalised profile of different materials within the TSF. A schematic representation of the Johnson Soil®, Thompson type, hand auger (75mm diameter) used for drilling is depicted in *Figure 20*. Disturbance of the natural material profile was considered to be of lesser importance as the material distribution and grading is anthropogenically created and uniform throughout each profile drilled. The chemical composition of the tailings material also remains unaltered as this is an unlubricated, low-impact drilling method.

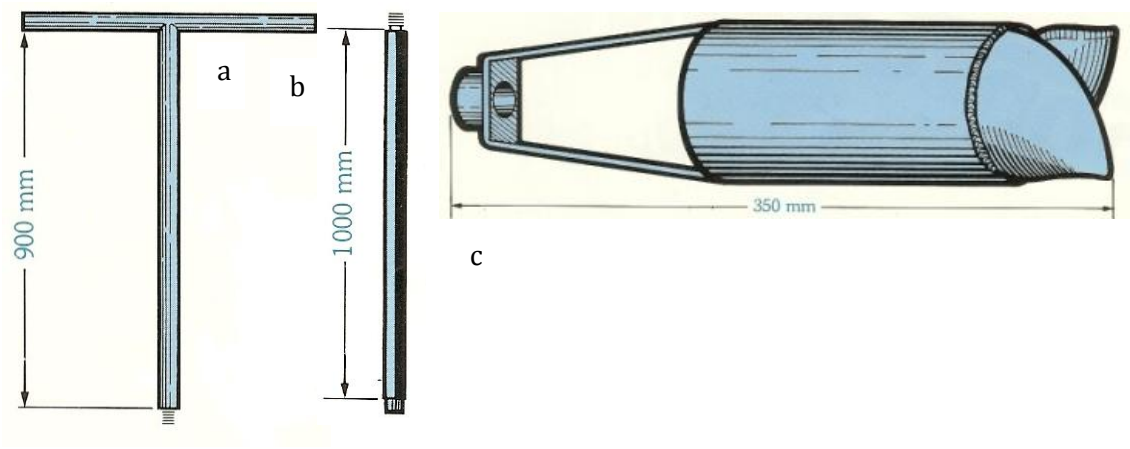

Figure 20: (a) Standard T- piece, (b) Auger extension rod, (c) Auger bucket head (Johnson Soil, 2011)

4.1.2 Direct Push Probe Drilling

Direct push probe drilling was employed to sample the tailings material in 2012. Although more expensive, this method provides undisturbed samples in PVC tubes and completely retains the material structure, moisture content distribution and chemical properties. This would provide even more detail on the conditions in the tailings material than that obtained by hand auger drilling. This method also provided a depth much greater than that reached by the hand auger sampling, down to soil level below the tailings facility.

The drill used is the AMS PowerProbe 9100VTR Diesel model, illustrated on the tailings facility in *Figure 21*. This rig uses its own static self-weight, combined with hydraulic down pressure and rapid hydraulic hammering to advance hollow stem augering equipment into subsurface lithologies.

Figure 21: Direct push probe drilling on the tailings storage facility on 20 February 2012.

Contained within the hollow stem auger equipment is a PVC tube of standard 1.2m length that is advanced into the subsurface material. When drilling has advanced 1.2m, the PVC tube is retracted with a sample of the material, an extra auger stem is added and a new PVC tube inserted. Drilling then continues to advance another 1.2m into the subsurface. This method is specifically designed to drill into- and sample soft sediments.

4.2 Sampling Locations

Samples were collected at the locations indicated in *Figure 22*. These four locations were chosen based on the constraints of spatial representation, accessibility and moisture content. Tailings material at these locations was moist enough to provide cohesion during extraction by hand auger drilling, but also dry enough to provide a safe, stable platform to drill on without the hole collapsing due to pore fluid pressures.

Auger holes were drilled into the top, middle and bottom terraces of the TSF in 2011 as indicated in *Figure 22*. These three locations provide a spatial representation of each cycle of tailings disposal forming the entire TSF.

The direct push probe hole was drilled in the terrace bank of the uppermost disposal terrace in 2012. This location was stable enough to allow the drill rig to remain stationary without sinking into the tailings facility. The samples obtained from this area would also represent the tailings in its entirety as a depth down to the original soil level could be reached with this drilling method. This would provide samples representing the very first tailings disposal up to the latest cycle of disposal.

Figure 22: Aerial photograph of the tailings storage facility indicating sampling positions

4.3 Sampling Depth and Frequency

Hand auger sampling of the tailings material in 2011 was performed with each advance of an auger bucket length i.e. 20cm. The samples collected and the extent of each are tabulated below in *Table 4*.

Table 4: Samples collected from the Tailings Storage Facility by Hand Auger

	TAH01	TAH02	TAH03
Sample Depth in Meters Below Groundlevel (mbgl)	0-0.2	0-0.2	0-0.2
	0.2-0.4	0.2-0.4	0.2-0.4
	0.4-0.6	0.4-0.6	0.4-0.6
	0.6-0.8	0.6-0.8	0.6-0.8
	0.8-1.0	0.8-1.0	0.8-1.0
	1.0-1.2	1.0-1.2	1.0-1.2
	1.2-1.4	1.2-1.4	Depth of refusal
	1.4-1.6	1.4-1.6	
	1.6-1.8	1.6-1.8	
	1.8-2.0	1.8-2.0	
	2.0-2.2	2.0-2.2	
	2.2-2.4	2.2-2.4	
	2.4-2.6	2.4-2.6	
	2.6-2.8	2.6-2.8	
	2.8-3.0	2.8-3.0	
	3.0-3.2	3.0-3.2	
	3.2-3.4	3.2-3.4	
	3.4-3.6	Excavation ceased	
	3.6-3.8		
	Excavation ceased		

Sampling was stopped in auger holes TAH01 and TAH02 after collapse, due to pore fluids, started to occur at the indicated depths of refusal in *Table 4*. Sampling was stopped in auger hole TAH03 after anorthositic gravel was encountered at the depth of refusal indicated in *Table 4* and further progress could not be made. Important points to note are:

- Samples from TAH01 were wet below 3.2 mbgl
- Samples from TAH02 were wet below 0.3 mbgl
- Samples from TAH03 were wet below 0.1 mbgl
- A stale, sulphuric smell was encountered at 2 mbgl in TAH02.

Samples were collected at the above-mentioned frequency to ensure a complete profile is represented and analyses performed yield complete results with minor to no gaps in the acquired data.

The direct push probe sampling in 2012 was a continuous sampling run with sample tubes being returned every 1.2 m of drilling. The samples collected and the extent of each are tabulated below in *Table 5*.

Table 5: Samples collected from the Tailings Storage Facility by Direct Push probe Drilling

	TPH
Sample Depth in Meters Below Groundlevel (mbgl)	0-1.2
	1.2-2.4
	2.4-3.6
	3.6-4.8
	4.8-6.0
	6.0-7.2
	7.2-8.4
	8.4-9.6
	9.6-10.0
	End of hole

Sampling was stopped due to the encountering of hard, anorthositic gravel at the bottom of the tailings, which was present in the underlying soil. Therefore, the PVC tube could not advance further without being damaged and causing a loss of sample material. However, a very complete profile of the tailings material, down to soil level, was obtained for the tailings material using this drilling method.

4.4 Sample Containment

The samples collected from the Tailings Storage Facility in 2011 were contained in 300 x 400 mm industrial plastic bags and sealed tightly with 100 mm plastic cable ties to retain the natural moisture content of the material. The direct push probe samples were contained in the original sampling tubes and sealed with wax paper and plastic caps at both ends to completely isolate the sample.

This prevents the material from desicating, clumping and hardening, making it more manageable to extract smaller samples from the bulk samples for analyses. Moisture content was also retained to preserve the in situ pH and Eh of the samples as far as possible, to ensure representative data obtained from any analyses performed on the material.

4.5 Analyses Performed

Different lab analyses and tests were performed on the tailings material sampled from the Tailings Storage Facility. This was done to determine the mineralogical composition, elemental composition, sulphide content, acid generation potential and contaminant leachability of the tailings material at different depths in the TSF. The methods employed are explained below.

4.5.1 Quantitative and Qualitative X-Ray Diffraction

The samples were prepared for XRD analysis using a back loading preparation method. They were analysed in the Department of Geology Analytical Facility of the University of Pretoria using a PANalytical X'Pert Pro powder diffractometer with X'Celerator detector and variable divergence-and receiving slits with Fe filtered Co-Kα radiation. The phases were identified using X'Pert Highscore plus software. The relative phase amounts (weight %) were estimated using the Rietveld method

(Autoquan Program). Errors are on the 3 sigma level. Amorphous phases, if present were not taken into consideration in the quantification.

4.5.2 X-Ray Fluorescence Spectroscopy

The samples were prepared as pressed powder briquettes. The ARL9400 XP+ Sequential XRF and Uniquant software was used for analyses in the Department of Geology Analytical Facility of the University of Pretoria. The software analysed for all elements in the periodic table between Na and U, but only elements found above the detection limits were reported. The values were normalised, as no LOI was done to determine crystal water and oxidation state changes. All elements were expressed as oxides.

4.5.3 Reflected Light Microscopy

Four samples obtained from the direct push probe samples were prepared as polished sections in the Department of Geology Analytical Facility of the University of Pretoria. These sections were petrographically analysed using an Olympus Petrographic Microscope connected to an external light source. The microscope has 5x, 10x and 50x magnification oculars available. Reflected light petrographic analyses were performed to identify oxide- and sulphide minerals in the samples which represented different depths in the tailings storage facility.

4.5.4 Acid-Base Accounting and Net Acid Generation Potential

In an Acid-Base Accounting analysis, two major parameters are quantified. These parameters are the acid generation potential and the acid neutralisation potential.

A tailings sample was submitted to WaterLab® in Pretoria where it was analysed for total sulphur content from which the percentage of sulphur present as sulphides were analytically calculated. The acid generation potential was calculated by multiplying the percentage of sulphur present as sulphides with a factor of 31.25 (Price, 1997). Acid generation potential is expressed as kg of $CaCO_3$ per ton of rock. This indicates the mass of theoretical calcite neutralised by the produced acid.

To calculate the acid neutralisation potential of the sample, a known volume of hydrochloric acid was added to the sample, followed by a titre of sodium hydroxide to determine the amount of unreacted acid. Acid neutralisation potential is also expressed as kg of $CaCO_3$ per ton of rock to represent the amount of theoretical $CaCO_3$ available in the rock material, to neutralise acid.

The net acid generation potential of the tailings material was then calculated by subtracting the acid neutralisation potential from the acid generation potential. A positive value indicates potentially acid forming rock whereas a negative value indicates potentially non-acid forming rock.

4.5.5 Acid Leach Tests and Inductively Coupled Plasma- Mass Spectroscopy

The acid leach test results were obtained by performing the UIS Analytical Laboratories® Acid Rain Test on the samples as received by the laboratory. A 100 g fraction of each sample was rotated for 18 hours in 2000 ml of carbonated water at a pH between 3.6 and 3.8. The solution was filtered after the extraction process and the pH value was measured before analysis. The solution obtained from each sample was analysed for trace elements with the Perkin Elmer Elan 6100 instrument using inductively coupled plasma- mass spectroscopy. The ions analysed in each solution were Ag, Al, As,

Au, B, Ba, Be, Bi, Ca, Cd, Co, Cr, Cu, Fe, Ga, Ge, Hg , K, Li, Mg, Mn, Mo, Na, Ni, Pb, S , Sb, Se, Si, Sn, Sr, Th, U, Ti, Tl, V, W, Zn, Zr, F, Cl, NO2, NO3, PO4, SO4 and results were expressed as milligrams of each element per 1000 ml of solution.

4.6 Hydraulic Testing

Hydraulic testing was performed on the tailings material and underlying aquifer in the form of permeameter tests and pumping tests respectively. These tests aid in the determination of contaminant movement velocities and directions in the TSF itself as well as in the aquifer. The calculated parameters and graphic analyses of data provide boundary conditions for flow and also aid in the characterisation of a source and pathway. This adds clarity to the prediction of possible receptors and where contamination might possibly migrate to if present. The test methods are described below.

4.6.1 Permeameter Tests

Two permeameter tests were performed on the tailings material to determine hydraulic conductivity. The tests were conducted for 8 hours as steady state flow was already established after 2 hours. The permeameter is illustrated in *Figure 23*. It was constructed using a calibrated rain gage; flexible PVC tubing with 10 mm diameter; 5 mm thick Perspex lids which were grooved; a 500 mm Perspex column of 5 mm thickness and an internal diameter of 150 mm; 8 marine grade turnbuckles; 2 mm thick steel cables; 2 valves to control flow and finally sealed with silicon to prevent any leakage. The Perspex column was filled with the tailings material which was premixed with water, after which additional water was added to ensure that the maximum degree of saturation possible was obtained. The column was sealed after insertion of the tailings and wall mounted to run the test.

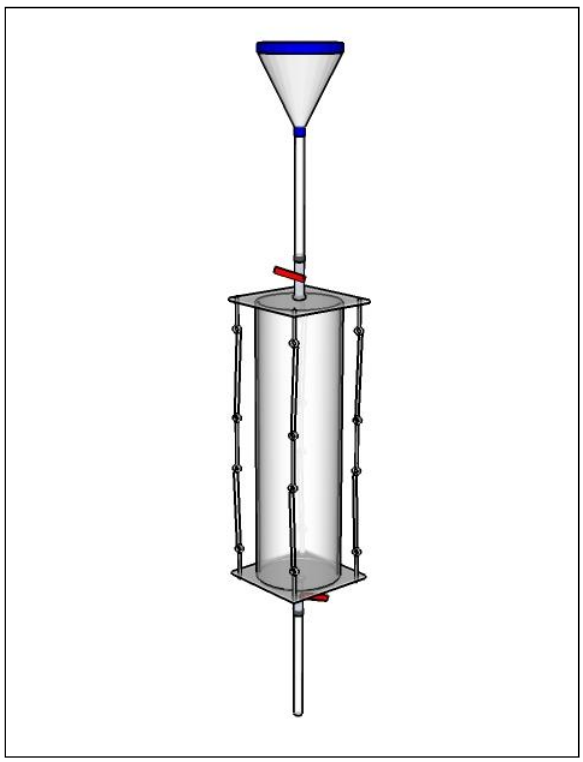

Figure 23: Schematic representation of the falling head permeameter used to obtain transport- and hydraulic properties of the tailings material.

4.6.2 Pumping Tests – AQTESOLV

Two pumping tests were conducted around the tailings storage facility between 14 and 16 March 2012 on existing monitoring wells to determine the hydraulic properties of the underlying aquifer. The tests were performed on two wells located between the tailings and the Steelpoort river which is considered to be a possible receptor of contamination. A pump was inserted to a depth where a known water strike was encountered during drilling as indicated by information received from the mine. The wells were pumped at a low discharge rate equal to the observed blow yield obtained during drilling, with waterlevel readings being noted at differing intervals to obtain high resolution data. This was performed using a TLC dipmeter. The low yielding wells were each pumped for a limited time period as steady state conditions were reached within 2 to 3 hours of pumping, and left to recover to a level as close as possible to the original datum waterlevel.

The data obtained from these tests were then interpreted using AQTESOLV software to determine the hydraulic parameters of the aquifer such as hydraulic conductivity, transmissivity, fracture depths, no flow boundary conditions as well as aquifer storativity. AQTESOLV is a software package used to analyse pumping tests, slug tests and constant-head tests.

4.7 Geochemical and Flow Modelling

The data collected from the field work, testing and analyses, were used to construct and calibrate geochemical and unsaturated flow models. The models were used to predict the future flow and chemical behaviour of the tailings, as well as to attempt to explain the processes that are currently taking place in the material. Each model and its application are explained in the paragraphs below.

4.7.1 Geochemical Modelling – The Geochemist's Workbench 9.0 Standard

The modelling software used to interpret the obtained geochemical data from the Tailings Storage Facility, is The Geochemist's Workbench® Standard 9.0 (GWB). As paraphrased from the developer's website (Rockware, 2011), The Geochemist's Workbench® is a set of software tools for solving water quality problems, including those encountered in environmental protection and remediation, the petroleum industry and mine wastewater planning. The software provides a platform for:

- Water data storage
- Unit conversion
- Evaluation of replicates and standards
- Flagging of exceedances
- Balancing chemical reactions
- Creating Pourbaix and activity diagrams
- Solution speciation calculations
- Mineral saturation calculations
- Gas fugacity calculations
- Predicting ion sorption and surface complexation
- Creating Piper, Stiff, series, time series, cross plot, ternary and other aqueous geochemistry diagrams
- Calculating polythermal and sliding fugacity reactions
- Incorporating mineral dissolution/precipitation kinetics and redox kinetics

- Specifying custom rate laws
- Modelling microbial metabolism and growth
- Obtaining Debye-Huckel or Pitzer activity coefficients
- Specifying flow-through and flush configurations
- Plotting flash (scaling) diagrams
- Modelling stable isotope fractionation.

The model was used to predict solution speciation of permeating fluids through the TSF as well as stable mineral phases that could potentially form. Rate constants for dissolution kinetics of existing, meta-stable mineral phases present in the tailings material were obtained from literature. The activities of different ionic species in the fluids permeating the TSF were also determined using activity coefficient equations available from the software.

4.7.2 Unsaturated Flow Modelling – HYDRUS

The modelling software was used to evaluate the unsaturated flow parameters of the tailings material is HYDRUS® 1D 4.0, a FORTRAN® based numerical unsaturated flow modelling software. This software can be used to calculate unsaturated hydraulic conductivities, vapour flow, heat flow and solute transport in variably saturated soil materials using the Richards equation.

As paraphrased from Šimůnek and van Genuchten (2009), the program may be used to analyse water and solute movement in unsaturated, partially saturated, or fully saturated porous media. The flow region may be composed of nonuniform soils. Flow and transport can occur in the vertical, horizontal, or a generally inclined direction. The water flow part of the model can deal with prescribed head and flux boundaries, boundaries controlled by atmospheric conditions, as well as free drainage boundary conditions. The governing flow and transport equations are solved numerically using Galerkin-type linear finite element schemes. This version of HYDRUS also includes a Marquardt-Levenberg type parameter optimization algorithm for inverse estimation of a variety of soil hydraulic and/or solute transport and reaction parameters from measured transient or steady-state flow and/or transport data.

5. RESULTS AND DISCUSSION

5.1 Analytical Results

The chemical results obtained for each analysis are interpreted and discussed in detail below and provide insight into different chemical and mineralogical aspects of the TSF-vadose zone-aquifer system.

5.1.1 X-Ray Diffraction

The X-Ray Diffraction analyses that were performed on the tailings material, took place at the StoneMan laboratory at the University of Pretoria. The analysis results are attached under Appendix A. The mineral phases present in the tailings material and underlying vadose zone are summarised below in *Table 6* and *Table 7* respectively.

Table 6: Mineral phases present in the tailings material on site

Mineral	Chemical Formula
Annite	$KFe_3(Al, Si)_3O_{10}(OH, F)_2$
Anthophyllite	$(Mg_{0.76}, Fe_{1.24})(Mg_{4.95}, Fe_{0.05})Si_8O_{22}(OH)_2$
Diopside	$(Ca, Mg)Si_2O_6$
Enstatite	$(Mg_{1.568}, Fe_{0.432})Si_2O_6$
Magnesiohornblende	$Na_{0.46}Ca_{1.7}Mg_{3.44}Fe_{1.72}Al_{1.08}Si_{6.92}O_{23}(OH)$
Lizardite	$Mg_3Si_2O_5(OH)_4$
Chromite	$NiCr_2O_4$
Anorthite	$CaAl_2Si_2O_8$
Talc	$Mg_3Si_4O_{10}(OH)_2$
Chlorite (Clinochlore)	$Mg_{5.1}Al_{1.2}Si_3Cr_{0.7}O_{10}(OH)_8$
Phlogopite	$KMg_3(Al, Si)_3O_{10}(OH,F)_2$
Muscovite	$KAl_3Si_3O_{10}(OH)_2$
Tremolite	$Ca_2Mg_5Si_8O_{22}(OH)_2$
Chalcopyrite	$CuFeS_2$

Table 7: Mineral phases present in the vadose zone on site

Mineral	Chemical Formula
Chlorite (Clinochlore)	$Mg_{5.1}Al_{1.2}Si_3Cr_{0.7}O_{10}(OH)_8$
Quartz	SiO_2
Kaolinite	$Al_2Si_2O_5(OH)_4$
Enstatite	$(Mg_{1.568}, Fe_{0.432})Si_2O_6$
Chromite	$NiCr_2O_4$
Anorthite	$CaAl_2Si_2O_8$

The variation in mineral content, as weight percentages, is graphically illustrated for each sample with depth in the figures below. These graphs display stacked totals with each colour representing a different mineral phase to illustrate the above mentioned variations, as well as the mineral abundances relative to each other for each assemblage at each sample depth. Material that was not accounted for and fall outside of the 1% error margin for accuracy may be present in the form of colloidal phases as XRD analysis only detects crystalline phases or analytical value rounding. Also, excess weight percentages may be due to analytical value rounding.

Figure 24 illustrates minor variations in enstatite, hornblende and anorthite abundances of up to 8%. This may be due to variations in the mineralogy of the hanging wall and footwall of the UG2, but may also indicate changes in different depositional cycles and mixing of material in a mostly uniform material. This figure also illustrates abundances of talc in excess of 5 weight% as well as the increase of the lizardite phase with depth. This figure represents the oldest cycle of tailings disposal at the facility.

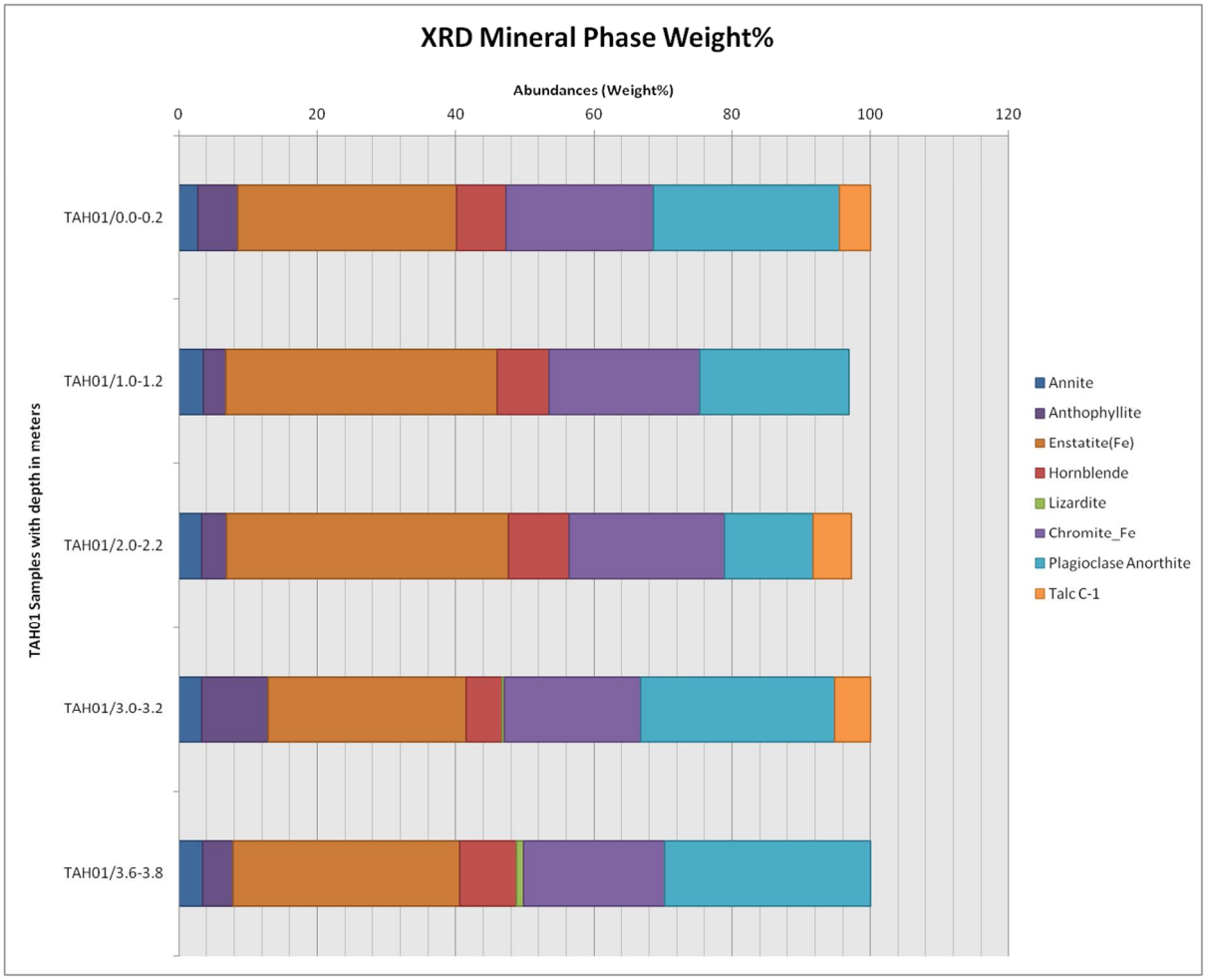

Figure 24: Mineral phase abundances with depth in TAH01

Figure 25 illustrates variations in enstatite, anorthite and hornblende as well as the complete replacement of the annite and anthophyllite phases with depth. The variations in enstatite and anorthite may be attributed to hanging wall and footwall variations in mineralogy during disposal cycles, but may also be a product of several different disposal cycles and mixing ratios. Lizardite can also be observed to be depleted within the first meter of the profile. This may indicate slightly older, more hydrated tailings material which has undergone more extensive weathering and dissolution present in the material during the deposition of this portion of the tailings profile. The depletion of annite and anthophyllite may be due to mineral structure changes with varying degrees of weathering, fluid content and oxygen availability in the rock before extraction. This could indicate the deposition of younger tailings material higher in the profile. At an approximate depth of 3 meters, annite can be observed to have been replaced with ferrian phlogopite which could be a result of magmatic mixing during the formation of the rock, changing this phase into its more Mg-rich end member phase. Magmatic mixing may also be responsible for diopside in the tailings at depth with Mg in the crystal structure of enstatite being substituted with Ca during the formation of a younger lava after its systematic depletion from the system. Its presence at depth in the tailings profile could therefore be explained by the mining of shallower, younger rock from the Critical Zone. This figure represents the second oldest cycle of tailings disposal.

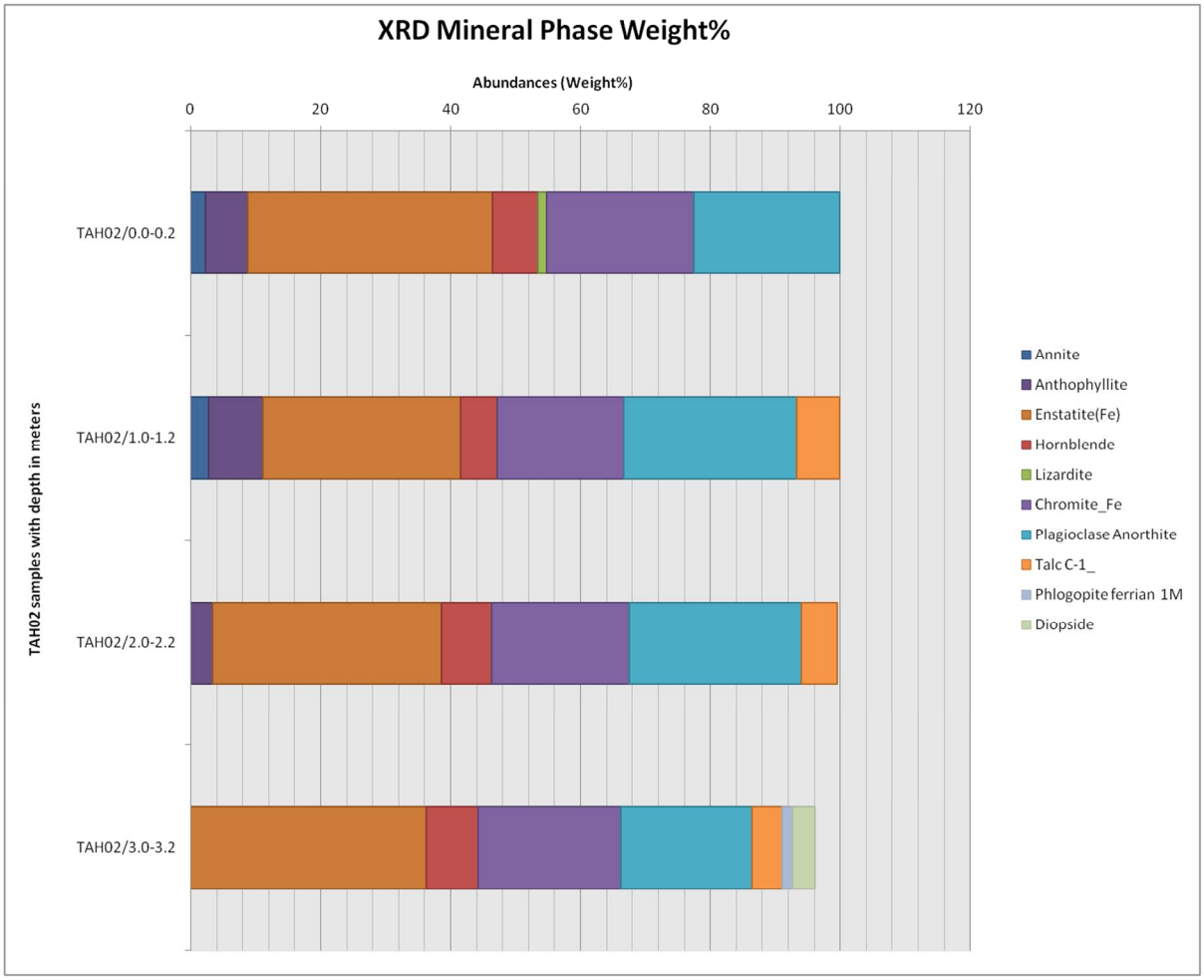

Figure 25: Mineral phase abundances with depth in TAH02

Figure 26 illustrates lesser variation in the enstatite phase with depth but much more so for the anorthite phase, as well as the complete replacement of the anthophyllite and diopside phases. This profile was obtained at the foot of the tailings, near a toedrain and variations may be due to material that has been transported from the tailings by geomorphic processes. The abundance of enstatite remains constant in each of the samples while diopside and anthophyllite is depleted. This is interpreted as differences in hanging wall and footwall mineralogy, as the profile does not show similar mineral abundance trends to the other two sampling localities where anthophyllite becomes depleted with the increase in diopside. However, this profile is interpreted to be extensively weathered as talc is an abundant phase with no lizardite present, as observed in the other profiles. Therefore, this profile is interpreted to have a mixed mineralogical signature and represents an area of mixing in the tailings material.

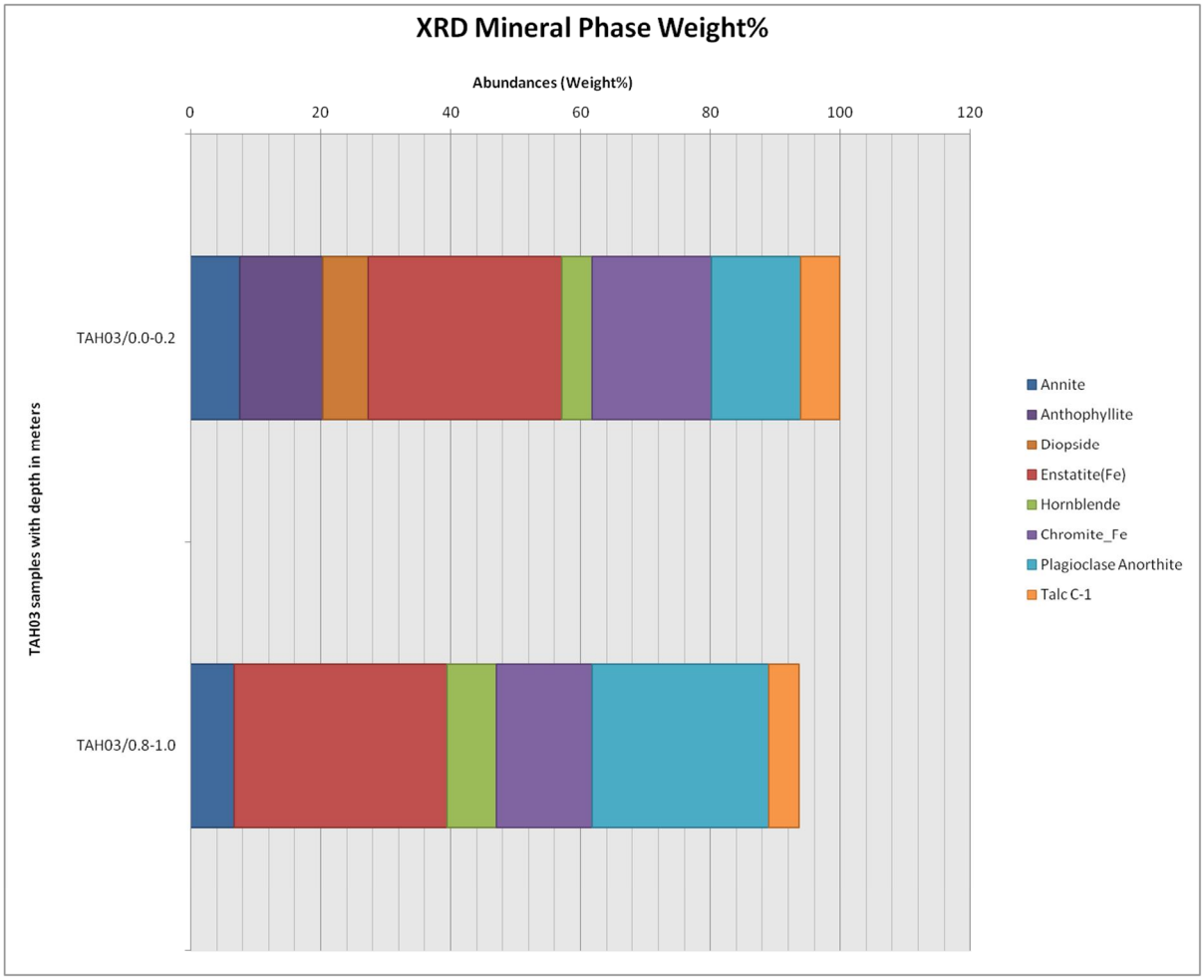

Figure 26: Mineral phase abundances with depth in TAH03

Figure 27 illustrates the mineral phase abundances in the direct push probe hole, drilled in the top terrace of the tailings as illustrated in *Figure 22*. Samples TPH0-1.2T to TPH8.4-9.6B represents tailings material from the top to the bottom of the TSF. Sample TPH9.6-10 represents the underlying soil material and natural vadose zone on site. From this figure, it is evident that throughout the TSF, the major composition of the material is an anorthite-enstatite-chromite assemblage with minor amounts of other mineral phases present. However, these phases are useful in interpretation of the origin and chemical evolution of the magmatic sequence throughout the profile, by acting as indicator minerals. Variations in enstatite and anorthite are inversely proportional to each other across the entire depth of the tailings profile. However, a point to be noted is that enstatite abundance is lower, shallower in the profile down to approximately 1.5 m and decreases abruptly at 8.4 m depth in sample TPH7.2-8.4B. This may have a skewing effect on the average mineralogical composition of the tailings but is interpreted as undulations in the reef and could possibly represent outliers in the data set due to a sudden localised change in reef composition. The higher abundance of quartz and kaolinite at this depth is explained as a zone of mixing in the tailings material between the tailings and natural soil material.

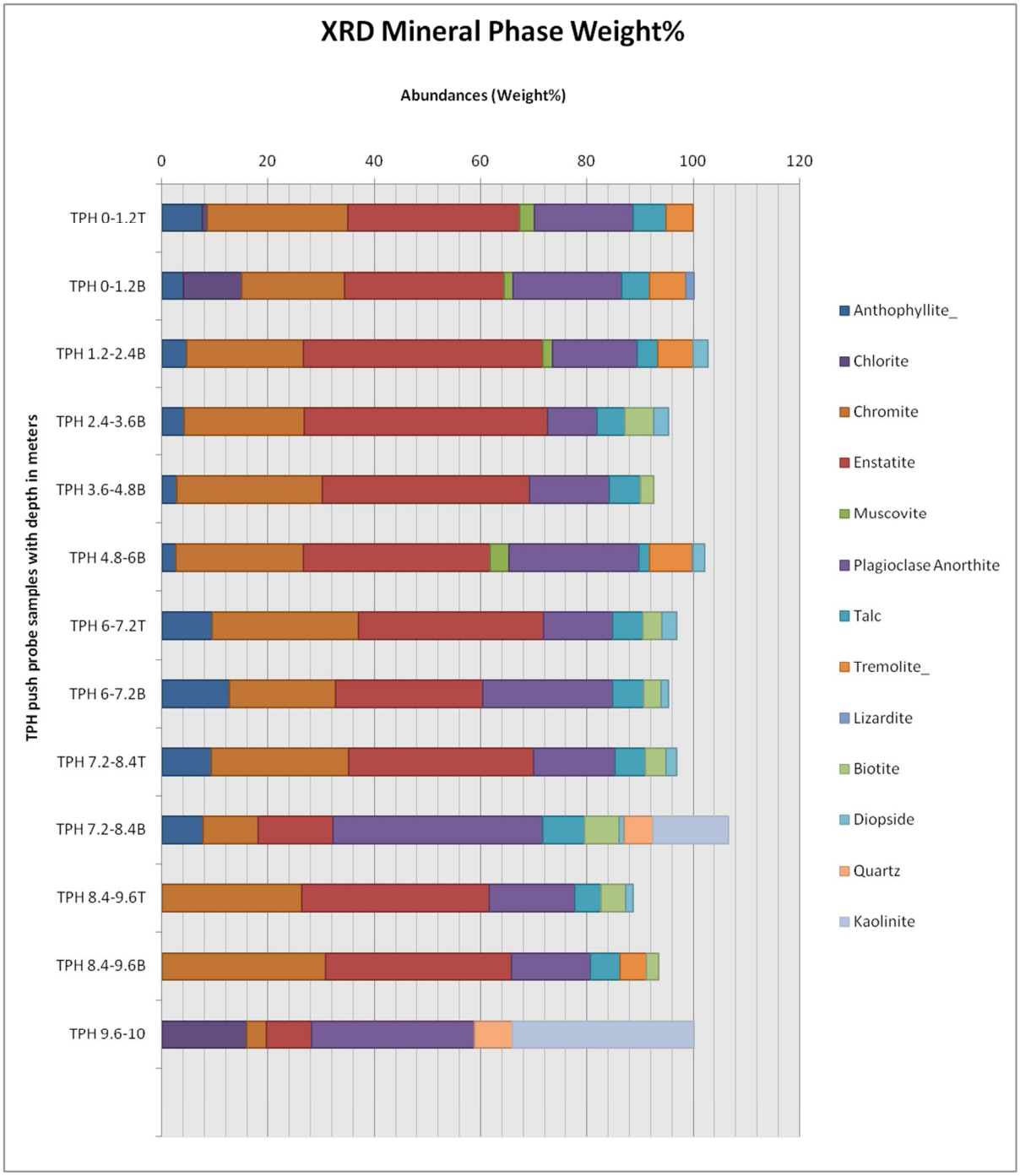

Figure 27: Mineral phase abundances with depth in TPH

Chlorite, muscovite and anthophyllite phases can all be observed to be minor phases in the tailings profile, linking with anomalous chemical compositions in the reef hanging wall and footwall due to various processes. The biotite and diopside phases increase with depth which is to be expected as these minerals decrease with depth as the mine progresses through the magmatic sequence from more intermediate to more mafic mineralogical assemblages. Talc and lizardite can also be found throughout the tailings profile, approximately inversely proportional to the abundance of the enstatite phase, which may indicate talc formation as a secondary mineral after enstatite breakdown by subsurface hydrothermal alteration. Another important point to note is that the weight percentage of chromite in each of the profiles discussed in this section showed little to no variation,

indicating its stability under a wide range of redox conditions as well as temperature and pressure conditions during the formation of the reef.

The mineral phases found in the soil profile constituting the natural vadose zone on site, predominantly consisted of anorthite, chlorite and kaolinite. Chlorite can be directly linked to the weathering of orthopyroxene minerals such as enstatite while kaolinite is a product of anorthite breakdown in the soil environment. Chromite was also found as a minor phase in the soil profile which may indicate mixing from tailings material. However, its low abundance may also indicate natural mixing from the underlying bedrock and its high resistance to weathering in the natural soil environment and redox conditions. Quartz is another minor mineral phase in the soil profile and is an abundant final product of the weathering cycle.

5.1.2 X-Ray Fluorescence Spectroscopy

The X-Ray Fluorescence analyses that were performed on the tailings material, took place at the Department of Geology Analytical Facility of the University of Pretoria. The major- and trace elements that were detected in the material were expressed as weight percentages in terms of oxides, tabulated below in *Table 8* and *Table 9* respectively. The analysis results are attached under Appendix B.

Table 8: Major element oxides as detected by XRF.

Major Element Oxides as Detected by XRF			
SiO_2	CaO	V_2O_5	CuO
TiO_2	Na_2O	ZRO_2	ZnO
Al_2O_3	K_2O	SO_3	Co_3O_4
Fe_2O_3	P_2O_5	WO_3	CeO_2
MnO	Cr_2O_3	BaO	SrO
MgO	NiO	Cl	MoO_3

Table 9: Trace elements as detected by XRF

Trace Elements as Detected by XRF			
As	Sr	Co	La
Cu	Th	Cr	Ce
Ga	U	F	Ba
Mo	W	S	Cl
Nb	Y	Sc	Rb
Ni	Zn	V	
Pb	Zr	Cs	

The variation in element oxide content, as weight percentages, is graphically illustrated for each sample with depth in the figures below. These graphs display stacked totals with each colour representing a different element oxide to illustrate the above mentioned variations, as well as the elemental abundances relative to each other for each assemblage at each sample depth.

Figure 28 illustrates variations in Si, Fe, Al, Mg, Ca, Cr and Na which are the most abundant major elements in the profile. Si decreases by 10% with depth up to 2.2 m where it starts to increase. Inversely proportionate to this element is the variations in Fe and Cr. Mg content stays relatively constant with Ca content following the same trend of variation as Si. This may indicate a direct link

to anorthite as the primary Ca bearing phase and may also control chromite stability to a certain degree as Cr weight percentages vary in an inversely proportionate manner to Si weight percentages.

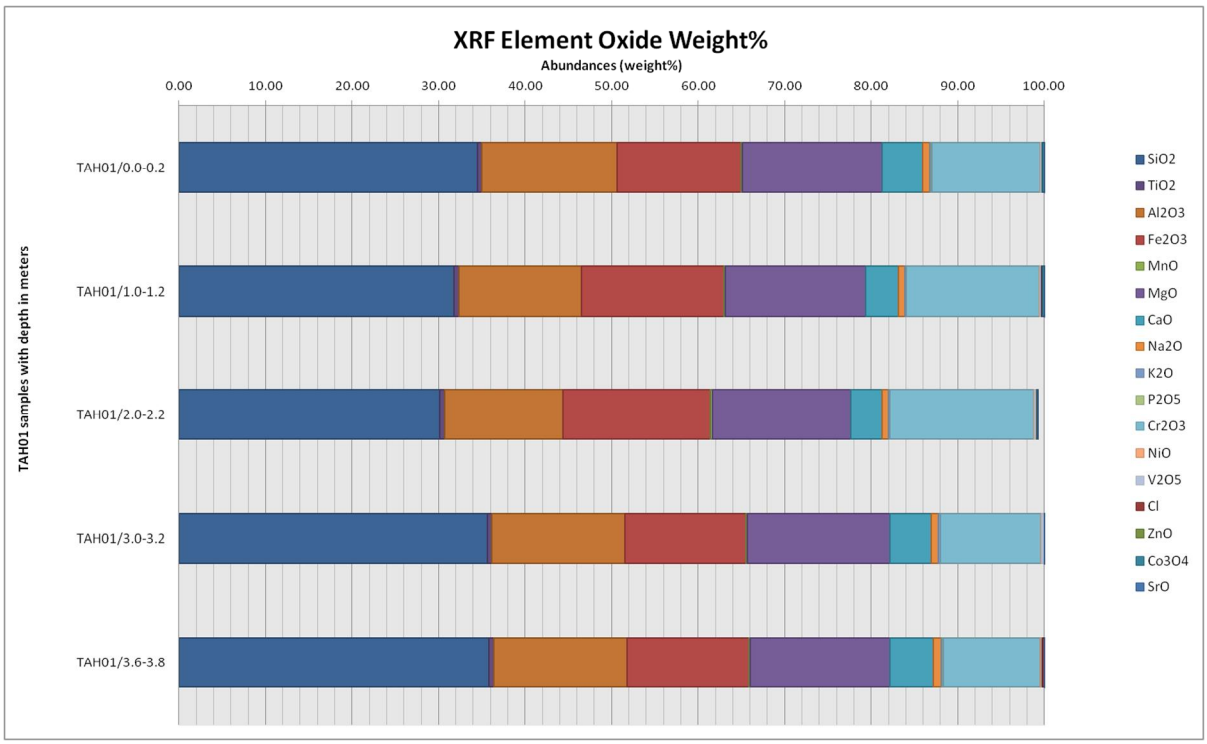

Figure 28: Element oxide abundances with depth in TAH01

Figure 29 illustrates a much more subtle variation in Si, Iron, Al, Mg, Ca, Cr and Na than that observed in TAH01. However, this figure illustrates the inversely proportionate relationship between Si and Cr content with Si content increasing slightly and then decreasing with depth. This may indicate a direct link to anorthite as the major Si bearing phase in the profile as its variation in abundance in this profile is much less pronounced. Fe, Al, Mg and Ca all remain approximately constant throughout the profile.

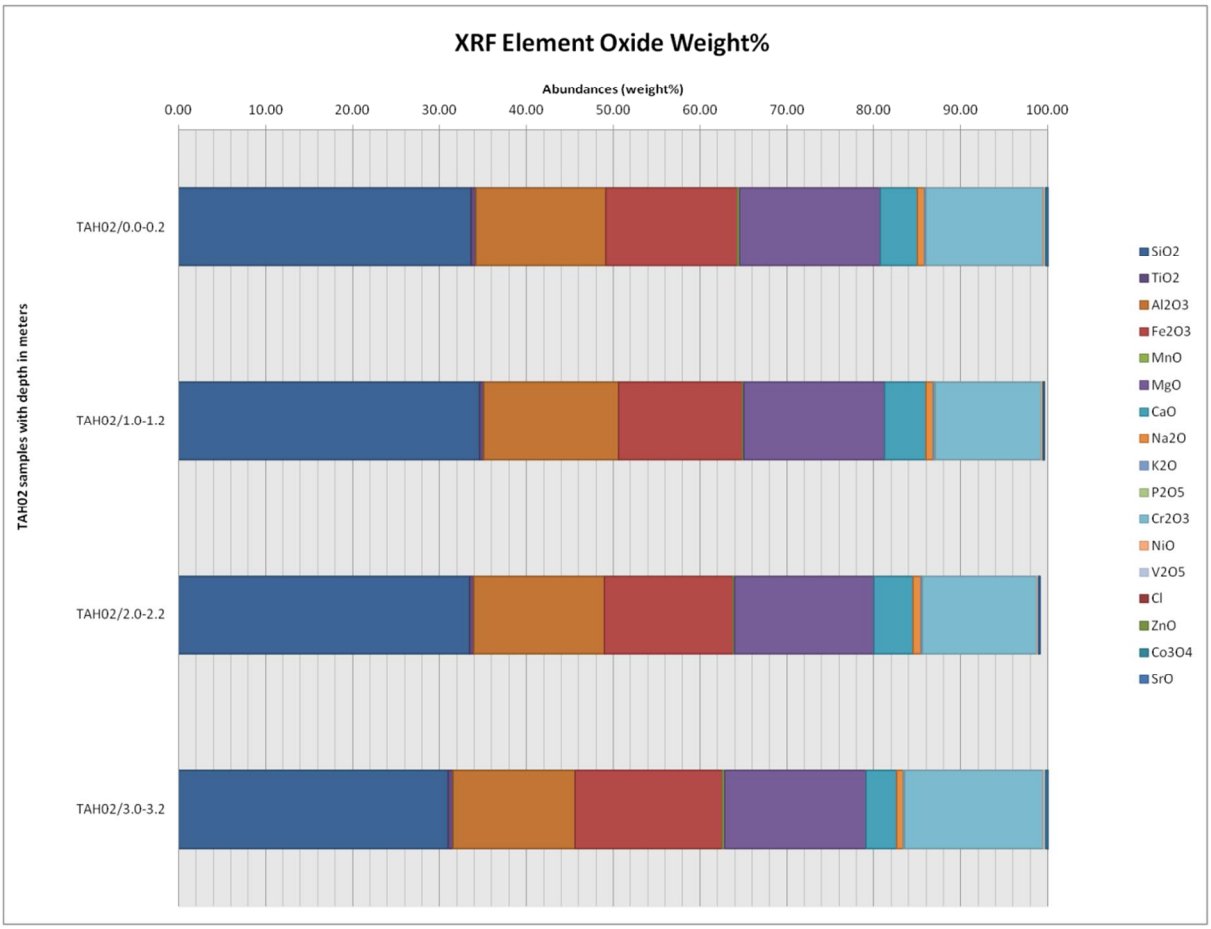

Figure 29: Element oxide abundances with depth in TAH02

Figure 30 illustrates more pronounced variations in Si content with depth and illustrates its inversely proportionate relationship with Cr much more obviously. Minor decreases in Fe content as well as Mg content can be observed with depth with increased Al content with depth. Therefore, chromite crystallisation may have been inhibited in the later stages of this magma which provided more suitable conditions for feldspar crystallisation, which is also indicated by the increase in Al and Ca content with depth.

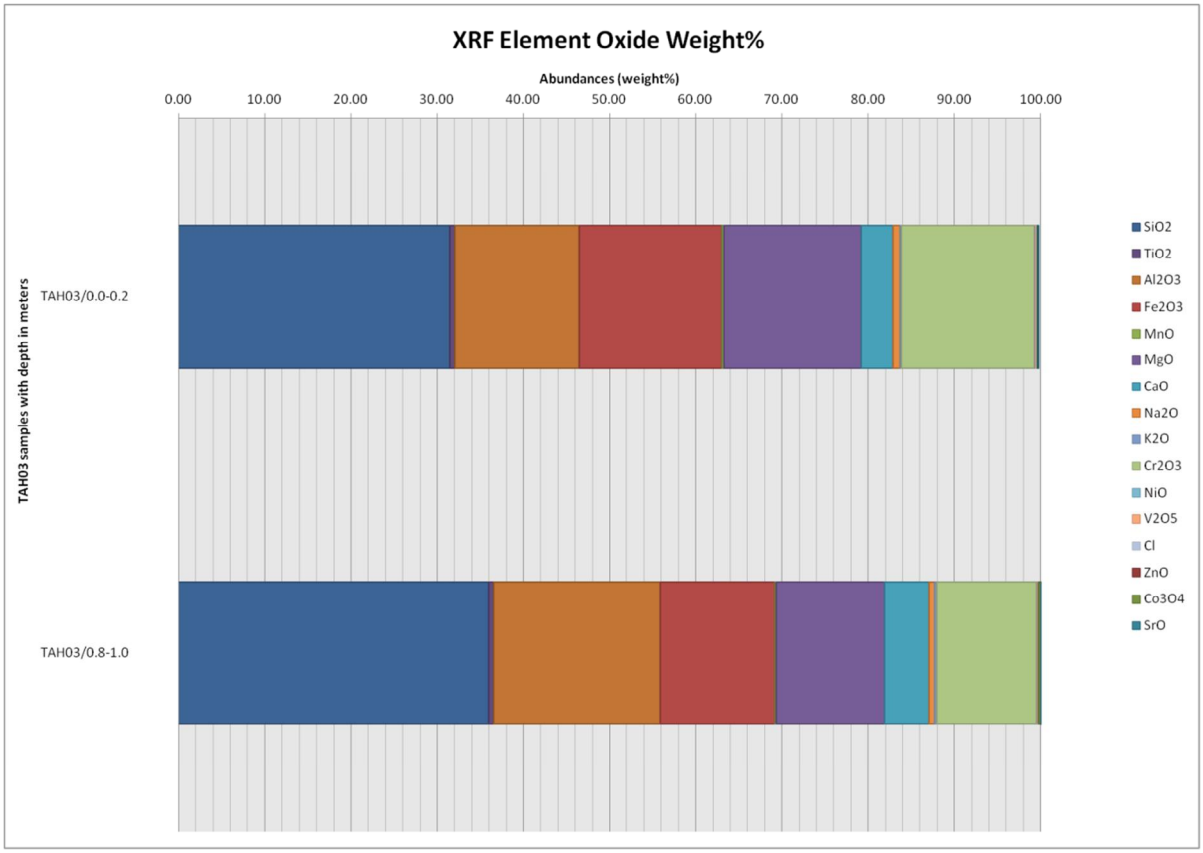

Figure 30: Element oxide abundances with depth in TAH03

Figure 31 illustrates major element oxides in the tailings material down to 9.6 m after which the major element oxides in the soil material comprising the natural vadose zone, are illustrated for depths between 9.6 and 10 m. The inversely proportional relationship between Si and Cr content is illustrated in this diagram, as well as throughout the tailings material down to soil level. The explanation given for this relationship for TAH03 also holds in this instance. An increase in Ca and Al content can also be observed at 9.6m which may indicate a higher abundance of anorthite. This could be because of increased enstatite weathering due to fluid ponding at this specific depth in the tailings material as enstatite is slightly more prone to weathering and dissolution than the anorthite phase. However, it is more likely that this is due to the mineralogy at shallower mining depths as well as mixing with the natural soil profile. In the rest of the tailings profile, Fe and Mg contents remain fairly constant. At soil level, Mg is almost entirely depleted with much lower Fe and Cr abundance and major increases in Ca, Al and Si. This may be attributed to long term weathering and pedogenesis, causing advanced breakdown and dissolution of the enstatite phase, with the remaining phases being constituted of secondary minerals and more felsic minerals, stripped of their once elevated Mg and Fe content.

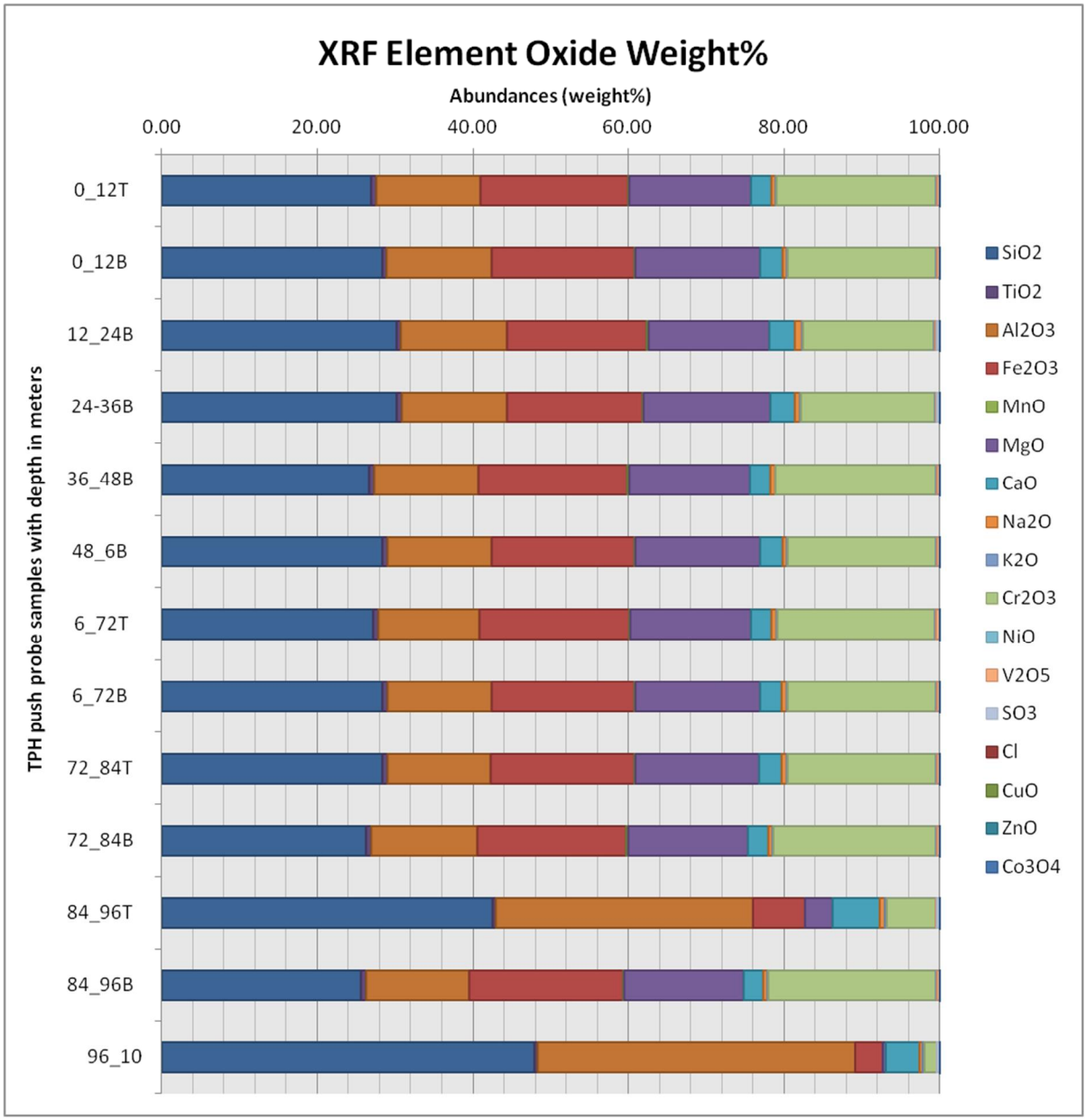

Figure 31: Element oxide abundances with depth in TPH

Figure 32 illustrates trace element oxides in the tailings material down to 9.6 m after which the trace element oxides in the soil material comprising the natural vadose zone, are illustrated for depths between 9.6 and 10 m. Zn, Ni and V variation can be observed to be directly proportionate to Cr variation throughout the profile indicating a direct link to chromite abundance in the profile. Ba and Cl abundance can be observed to be inversely proportionate to Ni abundance. This may indicate a link to silicate mineral phases such as anorthite which has approximately the same trend of abundance throughout the profile even down to soil level. The ratio of Rb to Sr and U may also indicate that the tailings material is variably saturated as Sr and U partitions readily into the fluid phase and these trace elements may have been concentrated in the material during the sample drying process. S can also be observed to follow an increasing trend with depth which may indicate significant decreases in oxygen to facilitate sulphide mineral dissolution. Cu can also be observed to remain approximately constant throughout the profile.

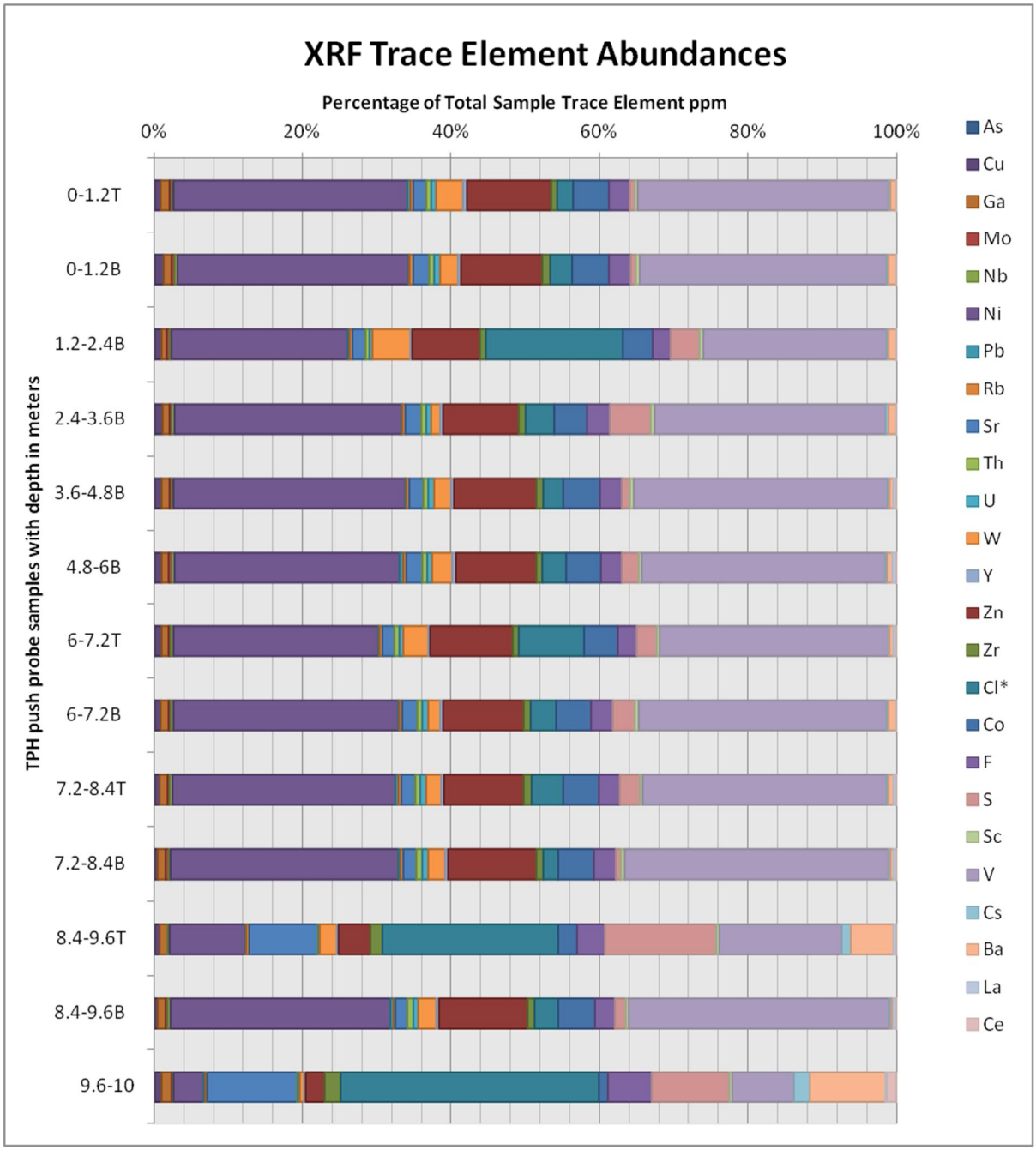

Figure 32: Trace element abundances with depth in TPH

5.1.3 XRF Element Correlations and Mineral Tracing

Figure 33 illustrates the correlation of specific trace elements with specific major elements from the XRD data discussed in the previous section. These elements were correlated to be able to observe a trend and attempt to link a certain trace heavy metal to a certain major ion which could then be linked to a specific mineral phase. Ca was correlated with Si and fitted with a linear trend line which fitted the data with an R^2-value of approximately 0.76 which is considered to be a moderately good fit. Si was found to be 5 times as abundant as Ca in the system. Anorthite and Diopside was concluded to be the major Ca bearing silicate phases in the system, with a ratio of one mol of Ca to 2 moles of Si each, based on abundances.

Al was correlated with Si and fitted with a linear trend line which fitted the data with an R^2-value of approximately 0.96 which is considered to be a good fit. Al was found to be 0.74 times as abundant as Si in the system. Anorthite, the biotite series, chlorite, muscovite and magnesiohornblende were identified as Al bearing phases. However, anorthite is the most abundant Al bearing phase and was therefore concluded to be the major Al bearing silicate phase in the system, with a ratio of 2 moles of Al to 2 moles of Si.

Mg was correlated with Si and fitted with a linear trendline which fitted the data with an R^2-value of approximately 0.91 which is considered to be a good fit. Si was found to be approximately 4 times as abundant as Mg in the system. Enstatite was concluded to be the major Mg bearing silicate phase in the system, with a ratio of 2 moles of Mg to 2 moles of Si, based on abundances.

Na was correlated with Si and fitted with a linear trendline which fitted the data with an R^2-value of approximately 0.67 which is considered to be a poor fit. Si was found to be approximately 12 times as abundant as Ca in the system. Due to the poor fit and correlation of the data, Na could not conclusively be traced to a specific silicate phase. However, the only XRD identified silicate phase containing Na is magnesiohornblende. Therefore, this phase may be a source of Na in tailings pore fluids. However, precipitated Na salts or amorphous phases may be more likely to be the source of Na based on the low abundance of the hornblende phase.

K was correlated with Si and fitted with a linear trendline which fitted the data with an R^2-value of approximately 0.8 which is considered to be a good fit. Si was found to be 130 times as abundant as K in the system which indicates only a slight positive correlation between these elements. The biotite series and muscovite was concluded to be the major K bearing silicate phases in the system, with a ratio of one mol of K to 3 moles of Si each. However, based on relative abundances and the correlation between these elements, the silicate phases cannot be conclusively isolated as the sole source of K and amorphous phases and K-rich precipitates are thought to be more likely sources of this element.

The trace heavy metals V, Co and Ni were all correlated with Cr. Each dataset was fitted with a linear trendline. Each trendline showed an R^2-value above 0.95 which is considered to be an excellent fit. Concentrations of Cr relative to these elements were found to be up to 544 times more abundant. However, based on the fit of the trendline to the data, the high correlation regression coefficient and chromite being the only Cr bearing phase in the system, it can be concluded confidently that these trace heavy metals are sourced from the chromite phase. An important point to note is that chromite is insoluble in most redox conditions as illustrated by the literature review section. Acidic conditions are required to dissolve this mineral phase and it may therefore pose a low contamination potential in terms of heavy metals.

Pb was also correlated with Cr abundances and fitted with a linear trendline which fitted the data with an R^2-value of approximately 0.23 which is considered to be a very poor fit. Therefore, Pb cannot be conclusively stated to be sourced from the chromite phase and could possibly exist in amorphous Pb-sulphide phases.

Cu was correlated with S and fitted with a linear trendline which fitted the data with an R^2-value of approximately 0.065 which is considered to be a very poor fit and that no correlation exists. However, the only Cu bearing phase in the system was found to be chalcopyrite which contains one mole of Cu for every two moles of sulphur. Therefore, the XRF data for these elements may not indicate a correlation of these elements, but petrographic data suggests otherwise.

Cu was then correlated with Fe in an attempt to illustrate the association with chalcopyrite. The data was fitted with a linear trendline which fitted the data with an R^2-value of approximately 0.23 which is considered to be an improvement but still a very poor fit. However, the only Fe bearing phase in the system containing one complete mol of Fe, was found to be chalcopyrite. Therefore, petrographic data again suggests otherwise.

Fe was then correlated with S in an attempt to illustrate the association with chalcopyrite. The data was fitted with a linear trendline which fitted the data with an R^2-value of approximately 0.15 which is considered to be a poor fit. However, the only Fe and S bearing phase in the system containing one complete mol of Fe and two moles of sulphur, was found to be chalcopyrite. Therefore, petrographic data suggests a possible alternative. Chalcopyrite is therefore suggested to be the main source of Cu, Fe and S species in the system.

Fe was correlated with Si and fitted with a linear trendline which fitted the data with an R^2-value of approximately 0.98 which is considered to be a good fit. However, a negative correlation between Si and Fe was observed, confirming the sulphide phase, chalcopyrite, to be the main source of this metal in the system. Pyroxenes and amphiboles were, however, not disregarded as iron contributors, but are thought to play a less significant role. *Figure 33* shows the correlations of the abovementioned results.

Figure 33: Correlation of major and trace element abundances obtained from XRF analysis.

5.1.4 Reflected Light Microscopy

Reflected light microscopy was performed on four polished sections, as tabulated in *Table 10*, at the University of Pretoria. This petrographic work was performed using an Olympus Petrographic Microscope with 5x, 10x and 50x magnification.

Table 10: Samples selected from different depths in the TPH direct push probe hole for reflected light microscopy

Selected sample for petrography	Sample depth
TPH1.2T	0.01m
TPH2.2.4B	2.4m
TPH6.7.2T	6.01m
TPH8.4.9B	9.6m

Figure 34 illustrates two grains of chalcopyrite identified in the entire polished section, prepared for the sample returned from a depth of 0.01 m. Each grain also shows a certain degree of alteration, indicative of active weathering processes which may have decreased the abundance of this mineral phase.

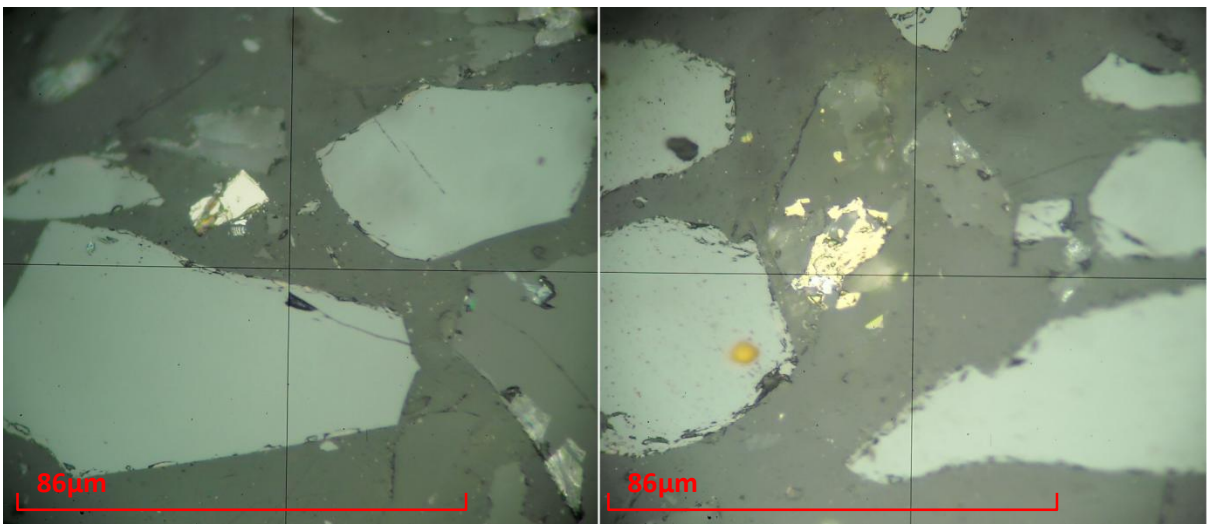

Figure 34: Reflected light microscopy images for sample TPH1.2T at 50x magnification.

Figure 35 illustrates pyrite (left) as well as chalcopyrite in a silicate phase (right). These are the only sulphide phases identified throughout the polished section, prepared from the sample returned from a depth of 2.4 m in the tailings material. The sulphide phases at this depth appear to be slightly more abundant with less alteration which may indicate a shorter exposure period to oxidising weathering conditions.

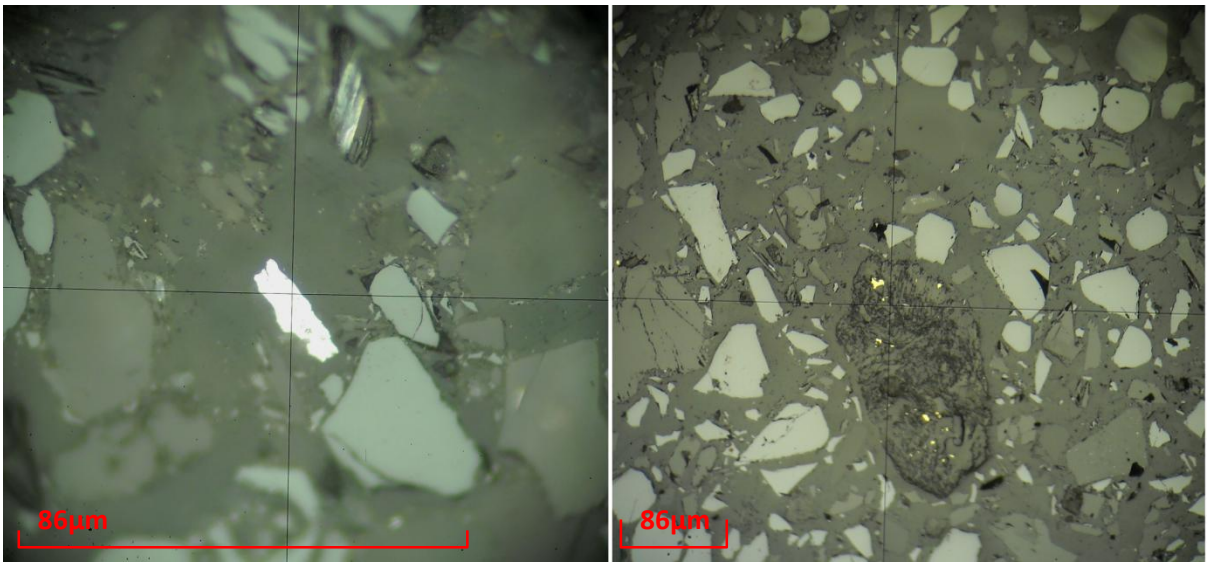

Figure 35: Reflected light microscopy images for sample TPH2.2.4B at 50x magnification (left) and 10x magnification (right).

Figure 36 illustrates a single occurrence of chalcopyrite throughout the entire section at 50x magnification. This section was prepared for the sample TPH6.7.2T, returned from a depth of 6.01 m in the tailings material. This grain appears to be unaltered by weathering which could be due to its isolation from oxygen at depth in the tailings. However, adjacent to it, a grain of chalcopyrite appears to be altered. This may be due to abundant fluids in the tailings material at this depth. However, this cannot be stated conclusively.

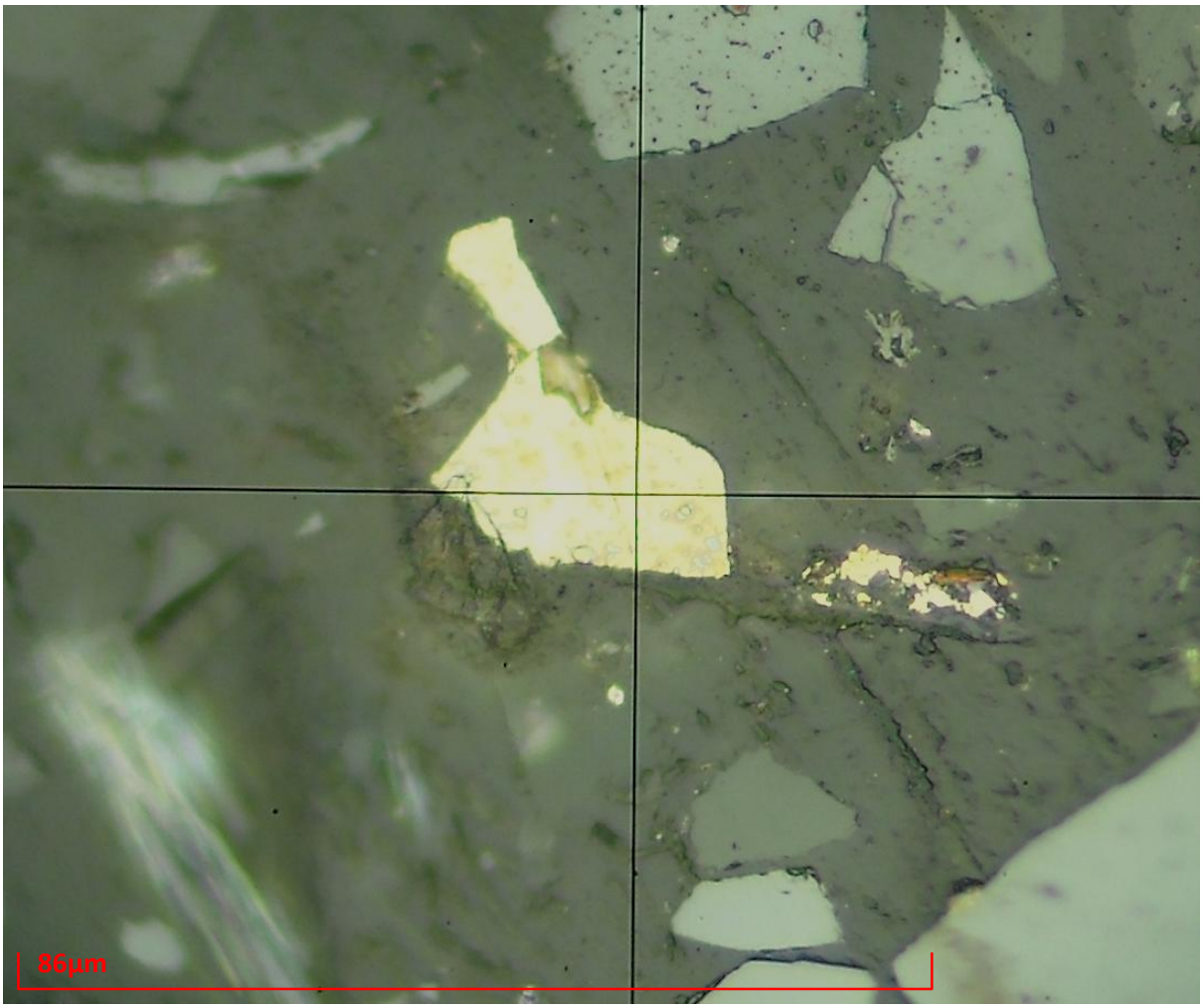

Figure 36: Reflected light microscopy image for sample TPH6.7.2T at 50x magnification.

Figure 37 illustrates single occurrences of pyrite (left) and chalcopyrite (right). These are the only occurrences of sulphide phases in the entire section, which was prepared from the sample extracted from 9.6m depth, in the tailings material. Both grains appear to be completely unaltered, indicating the highly anoxic conditions at the base of the TSF.

The abundances of sulphide phases in the tailings can therefore be concluded to be low, based on the microscopy images discussed in this section.

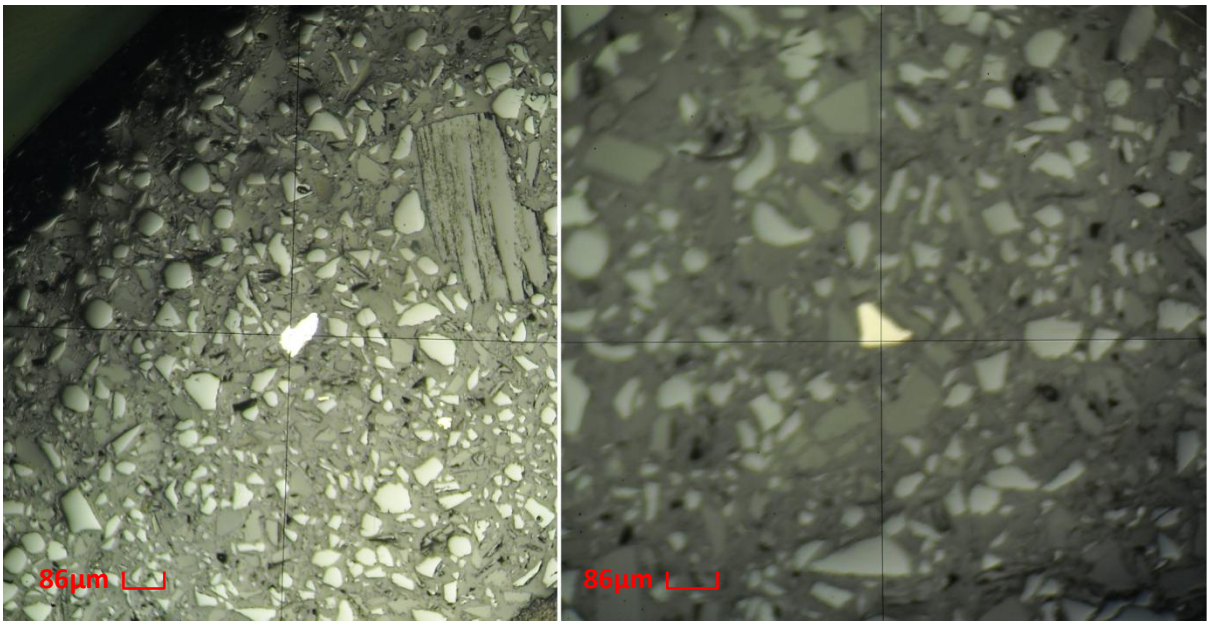

Figure 37: Reflected light microscopy images for sample TPH8.4.9B at 10x magnification.

5.1.5 Acid-Base Accounting and Net Acid Generation Potential

Acid-base accounting was performed at Waterlab® laboratories in Pretoria. The findings of the analysis are summarised below in *Table 11*. A duplicate sample, 4114D, was also tested to ensure reproducible results.

Table 11: Acid-Base Accounting Laboratory Results

Acid – Base Accounting Modified Sobek (EPA-600)	Sample Identification	
	Vadose Zone Hydrology TRPTS 1	Vadose Zone Hydrology TRPTS 1
Sample Number	4114	4114D
Paste pH	6.1	6.1
Total Sulphur (%) (LECO)	0.02	0.02
Acid Potential (AP) (kg/t)	0.62	0.62
Neutralisation Potential (NP)	8.50	9.50
Nett Neutralization Potential (NNP)	7.88	8.88
Neutralising Potential Ratio (NPR) (NP : AP)	13.73	15.34

The paste pH detected for the sample during acid-base accounting was 6.1. This indicates the pH of a sample mixed with distilled water to form a paste that has a liquid to solid ratio of 1:1. This indicates a slightly lowered pH that may be existent in the tailings at present. However, due to the nature of the test being performed over one hour, the paste pH value may be slightly skewed due to the time dependant reaction rates of sulphides and sulphates in the material, possibly generating acid in this time frame.

The total percentage sulphur in the sample was analysed with a LECO analyser and found to be 0.02%. The acid generation potential was calculated to be 0.062 kg of acid per ton of rock. This was calculated by multiplying the total percentage of sulphur by a factor of 31.25. The neutralisation potential was calculated, after treatment of the sample with a known volume of HCl and back-

titrating it with a known volume of NaOH. This determines the amount of unconsumed acid and the neutralisation potential of the rock can then be expressed as kg $CaCO_3$/ton of rock. This represents the theoretically available amount of calcite available in the rock, to neutralise acids.

The nett neutralisation potential was calculated by subtracting the acid generation potential from the neutralisation potential. This was found to be 7.88 kg $CaCO_3$/ton of rock in excess. The neutralisation potential ratio was found to be positive in the sample as well as in the duplicate sample at an average of 14. This indicates an unlikely ability of the rock material to generate acid. According to Price (1997) the tailings material is not potentially acid generating unless significant preferential exposure of sulphides exist, or extremely reactive sulphides in combination with insufficient reactive acid neutralisation potential are present.

5.1.6 Acid Leach Tests

Acid leach tests were performed on the tailings material collected from the auger holes. These analyses were performed on 18 August 2011 by Waterlab® laboratories in Pretoria. The leachable elements that were analysed for are listed below in *Table 12*.

Table 12: Elements analysed for during acid leach tests conducted in August 2011

Elements Analysed for in Leachate from Acid Leach Test					
Ag	Ce	Ho	Nb	Si	W
Al	Co	In	Nd	Sn	Y
As	Cr	Ir	Ni	Sr	Zn
Au	Cs	K	P	Ta	Zr
B	Cu	La	Pb	Te	F
Ba	Fe	Li	Pt	Th	Cl
Be	Ga	Mg	Rb	Ti	NO_2
Bi	Ge	Mn	Sb	Tl	NO_3
Ca	Hf	Mo	Sc	U	PO_4
Cd	Hg	Na	Se	V	SO_4

Leach tests were performed on each of the samples collected from the auger holes drilled in 2011 and the abundance of detected elements from the analyses are graphically illustrated below. *Figure 38* illustrates the abundances of the cations leached from samples collected from TAH01 during the acid leach tests. Ca, Mg, Na and Si were found to be the main leachable cations from the samples collected from this auger hole. It can also be observed that the abundances of these leached elements gradually increase with depth. This is a strong indication of the oxygen availability in the profile which may facilitate weathering and dissolution. Oxygen is illustrated to be depleted with depth in this profile as less weathering has taken place. This idea is supported by the abundances of leachable cations markedly increasing with depth, indicating that these elements may still be intact in less weathered mineral phases and also illustrates the accumulation of elements in pore fluid with depth. However, this could also be a function of additional mineral precipitates from permeating fluids in the tailings.

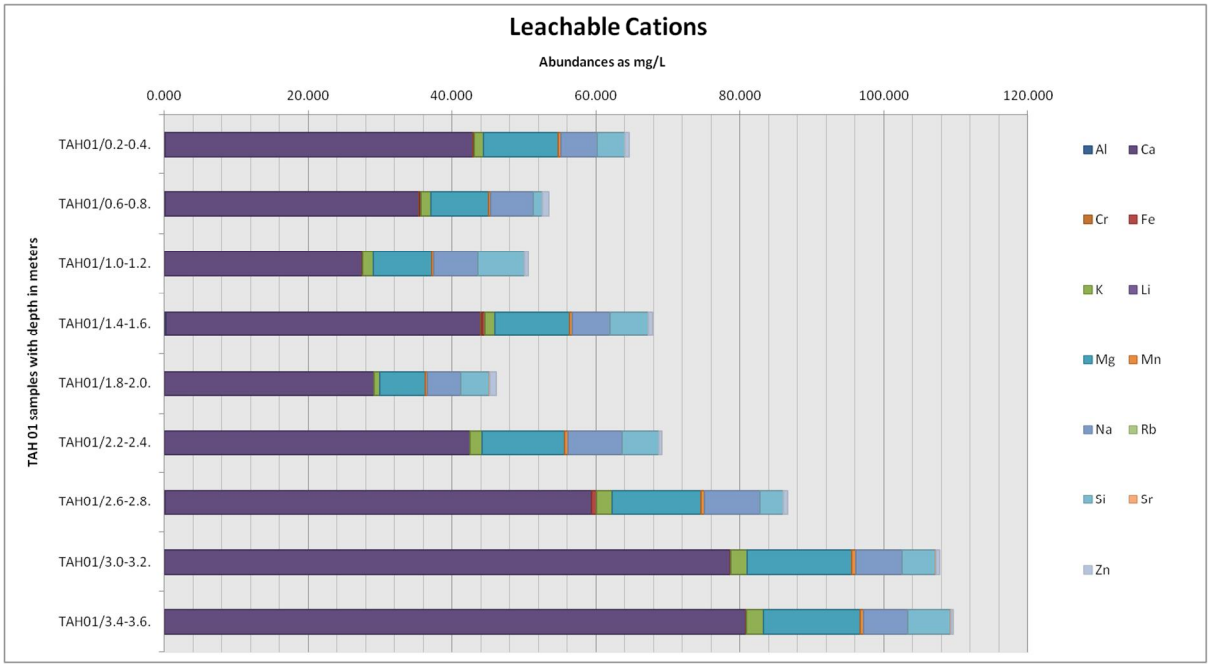

Figure 38: Leachable cations in samples collected from TAH01.

A corresponding graph for the leachable anions in the profile can be observed in *Figure 39*. This figure illustrates the leachable anion abundances from the same samples. However, the general trend of leachable elements does not indicate increasing abundances with depth. Nitrate concentrations decrease with depth and may be due to evaporative and desiccation effects with more nitrate available shallower in the profile. Other anion abundances remain fairly constant with variable amounts of sulphate being released. The concentrations of sulphate released may be an indication of changes in reef mineralogy during the material deposition cycle on the TSF. Leachable sulphate concentrations, however, do not indicate a clear trend in changing redox conditions in this profile.

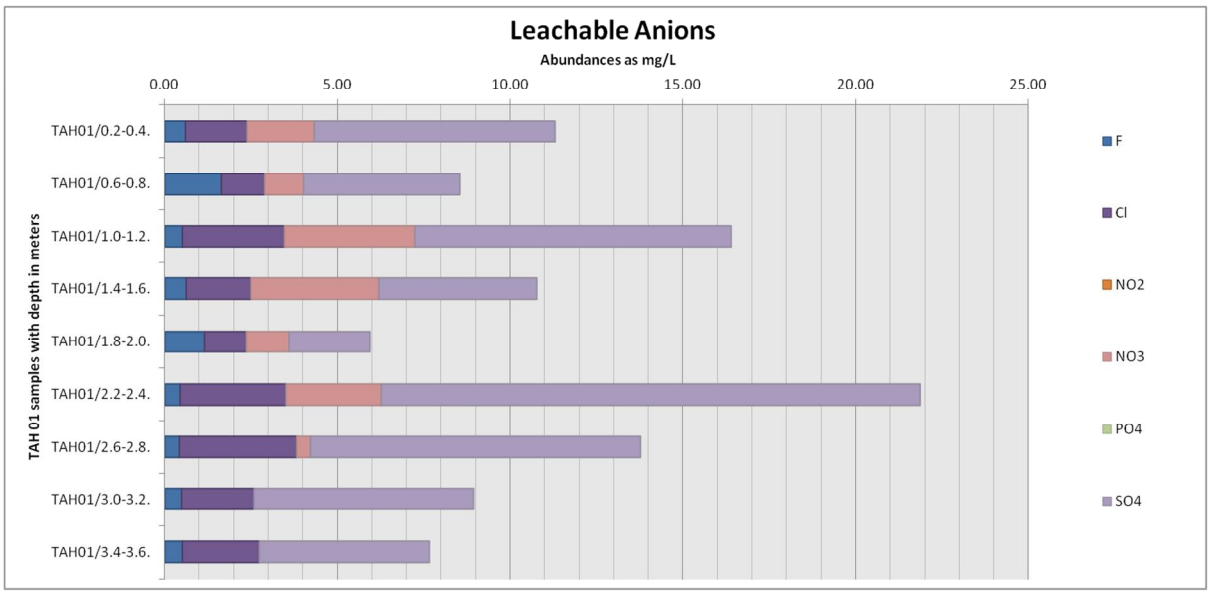

Figure 39: Leachable anions in samples collected from TAH01.

Figure 40 illustrates the abundances of the cations leached from samples collected from TAH02 during the acid leach tests. In this profile, Ca, Na, Mg and Si are also the main leachable elements. However, this profile does not supply clear information on the prevailing redox conditions as concentrations of these cations vary in an apparently random manner and do not indicate a trend of oxygen availability in the profile.

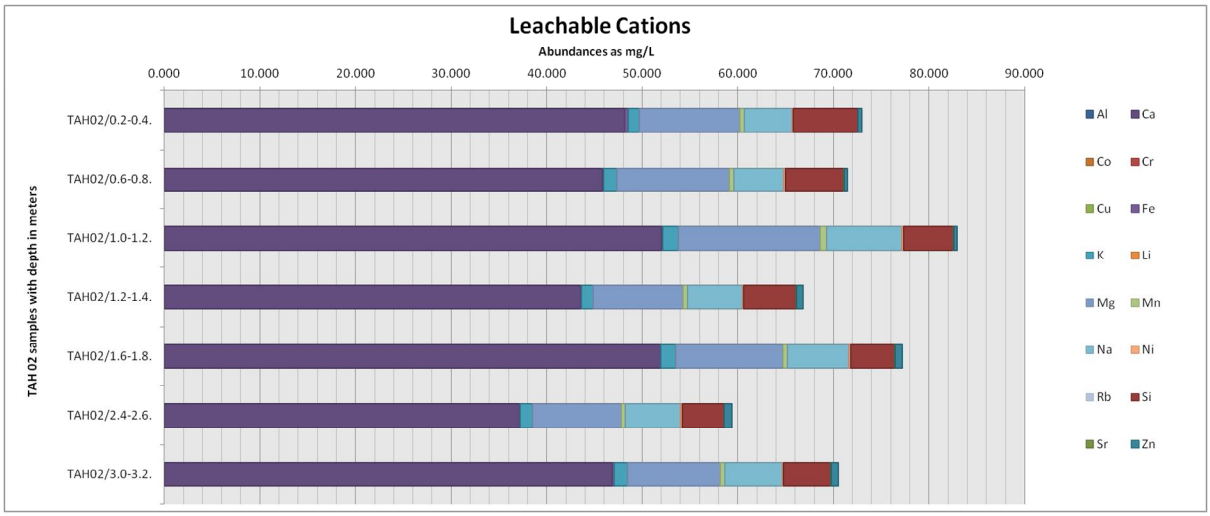

Figure 40: Leachable cations in samples collected from TAH02.

Figure 41 illustrates a corresponding graph indicating the leachable anions from the samples collected from TAH02. This graph illustrates no nitrate present which may indicate that the tailings material in this area has remained saturated for an extended period of time inhibiting nitrate precipitation from evaporative processes. Sulphate release is also variable throughout the profile and does not indicate a specific trend in redox conditions or oxygen content in the tailings material. Cl-abundances however, may reflect a fairly constant composition of the tailings material throughout this profile as the release concentrations of this conservative ion, remains fairly constant. This may indicate a saturated profile.

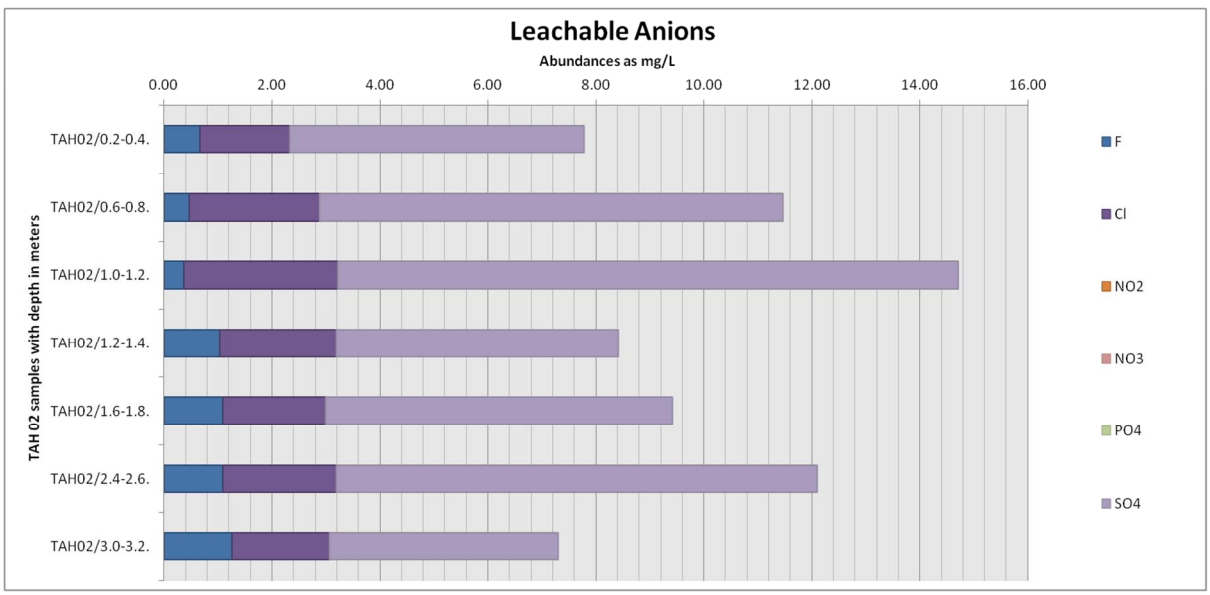

Figure 41: Leachable anions in samples collected from TAH02.

Figure 42 illustrates the abundances of the leachable cations from the samples collected from TAH03. The main leachable cations in this profile were found to be Ca, Mg, Na and Si. However, this profile illustrates the increased abundance of leachable elements with depth, indicating redox conditions changing from oxidising to reducing. This idea may indicate more weathered material shallower in the profile with fresher and less weathered material deeper in the profile, subsequently accompanied by more and less leachable ions respectively as well as increased cation concentrations in deeper pore fluids that may have accumulated over time.

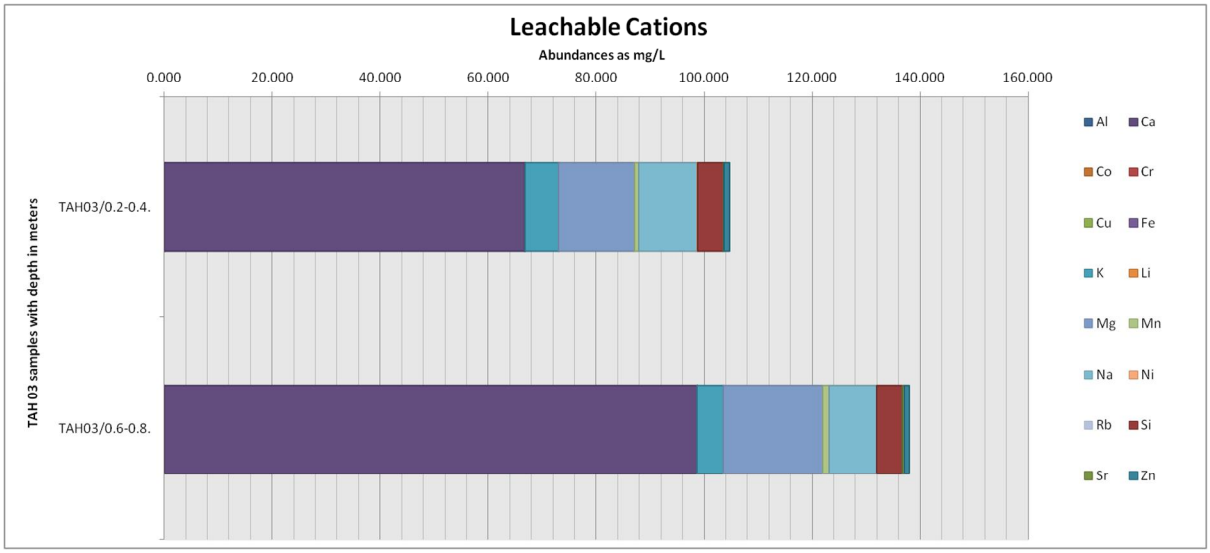

Figure 42: Leachable cations in samples collected from TAH03

Figure 43 illustrates a corresponding graph indicating the leachable anion abundances in the samples collected from TAH03. In this figure, more Cl and F are observed in the shallower part of the material which may indicate precipitation from evaporative processes as observed in *Figure 39* with nitrate abundances. This may indicate rapid evaporation and desiccation, subsequently increasing anion precipitation. However, the abundance of sulphates remains constant throughout the profile which may indicate relatively constant oxygen activity in the profile.

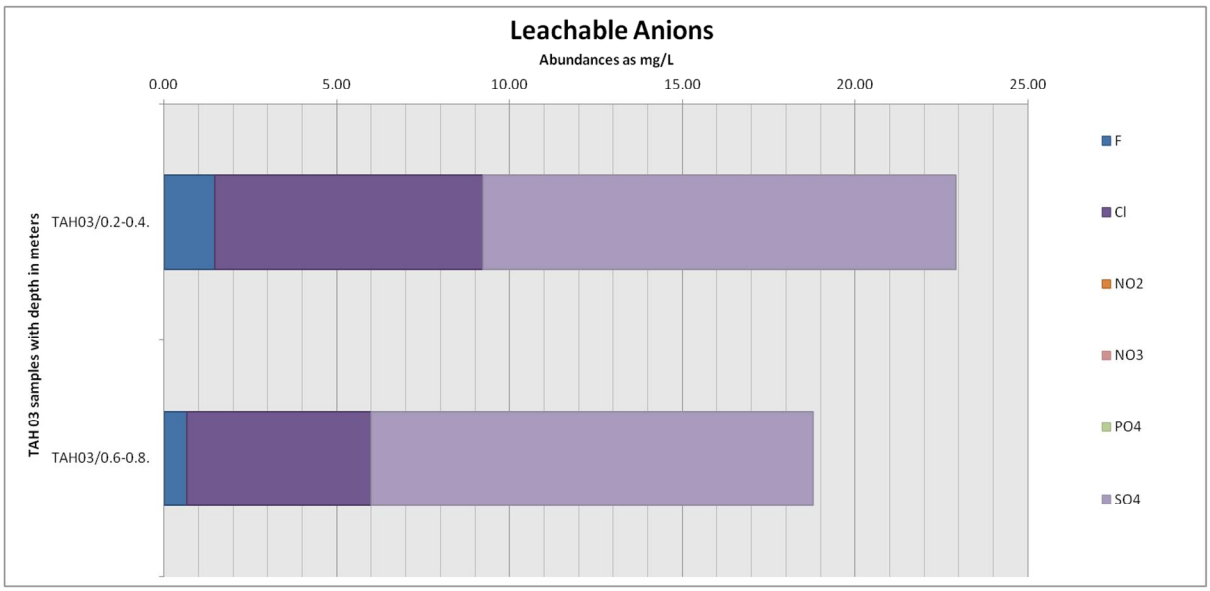

Figure 43: Leachable anions in samples collected from TAH03.

5.1.7 Inductively Coupled Plasma Scans

Water samples were collected from the toedrain of the tailings facility, two adjacent monitoring wells as well as the Steelpoort river during March and April of 2012. These samples were submitted to Waterlab® laboratories in Pretoria for inductively coupled plasma- optical emissions spectroscopy analyses. The results of the analyses are attached under Appendix C and are graphically illustrated in *Figure 44*.

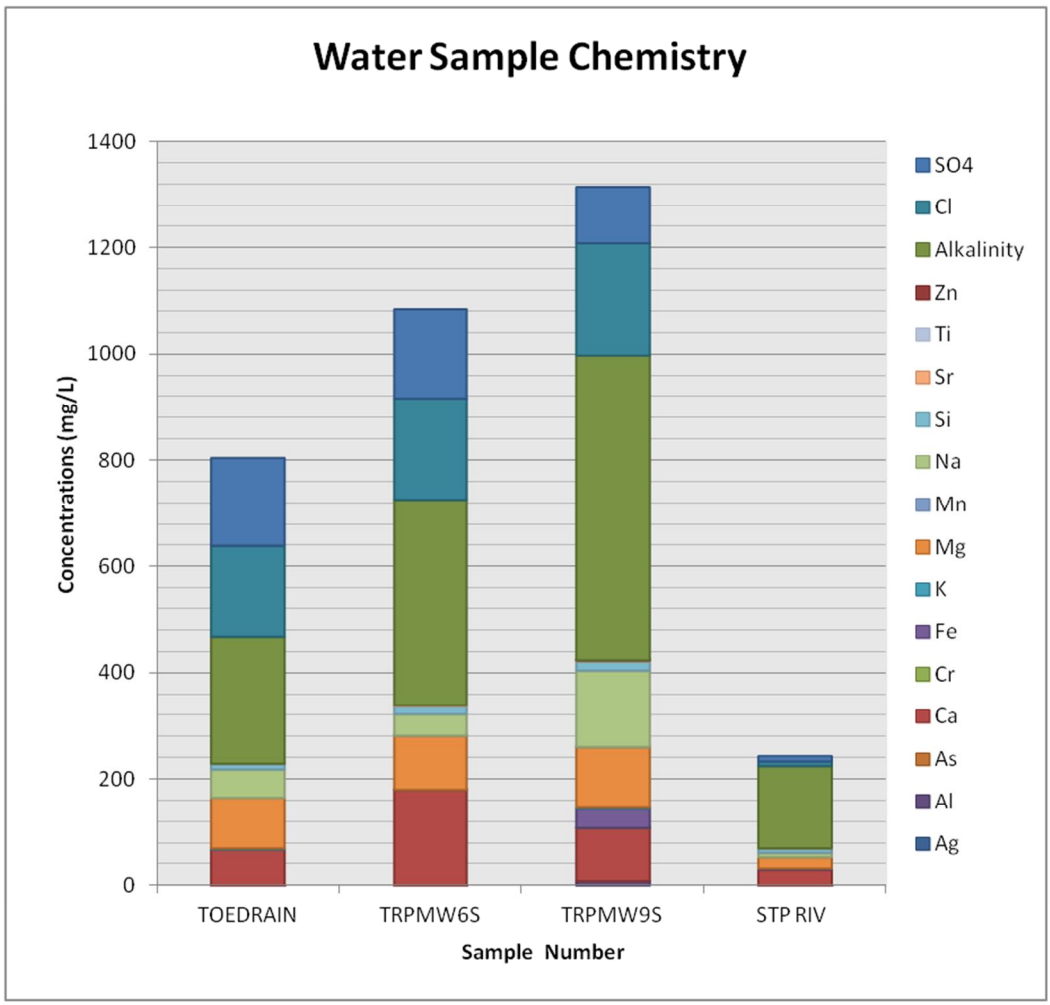

Figure 44: ICP-OES analysis results for collected water samples.

The sample TOEDRAIN was collected from a toedrain of the TSF to give a direct indication of the composition of fluids permeating the tailings. This sample was especially useful in the validation of geochemical models. The samples TRPMW6S and TRPMW9S were collected from shallow monitoring wells between the TSF and the Steelpoort river. Chemical data from these boreholes were expected to give an indication of the chemical evolution of hydro-chemistry in this area, following the drainage direction of the groundwater. The sample STP RIV was collected from the Steelpoort river west of the TSF. The chemical data obtained from this sample would give an indication if any contamination reached the river by groundwater flow and if the river is impacted by this contamination, making it a receptor. The water sampling locations are illustrated in *Figure 45*.

Figure 45: Water sampling positions around the tailings storage facility

Figure 46 illustrates stiff diagrams constructed using the major cation and anion concentrations in the water samples. From these diagrams, it can be observed that Ca and Mg are the most abundant cations in solution but show an abrupt decrease in the STP RIV sample. Abundant anions in each sample are CO_3 and HCO_3. These anions increase with distance from the tailings and are also indicated as alkalinity in *Figure 44*. However, Cl decreases steadily with distance from the tailings and abruptly decreases in the STP RIV sample. The same trend can be observed for SO_4.

Stiff diagrams act as a fingerprint to identify a specific water type. Similar diagrams or logical chemical evolution between diagrams may indicate a link between different samples, indicating a similar chemical fingerprint for each water sample. This may indicate a link between- or similar source area for each water sample. These diagrams appear to show a link between groundwater and surface water in this area with a large dilution factor present in the river, as a logical chemical evolution of the major ions takes place with distance.

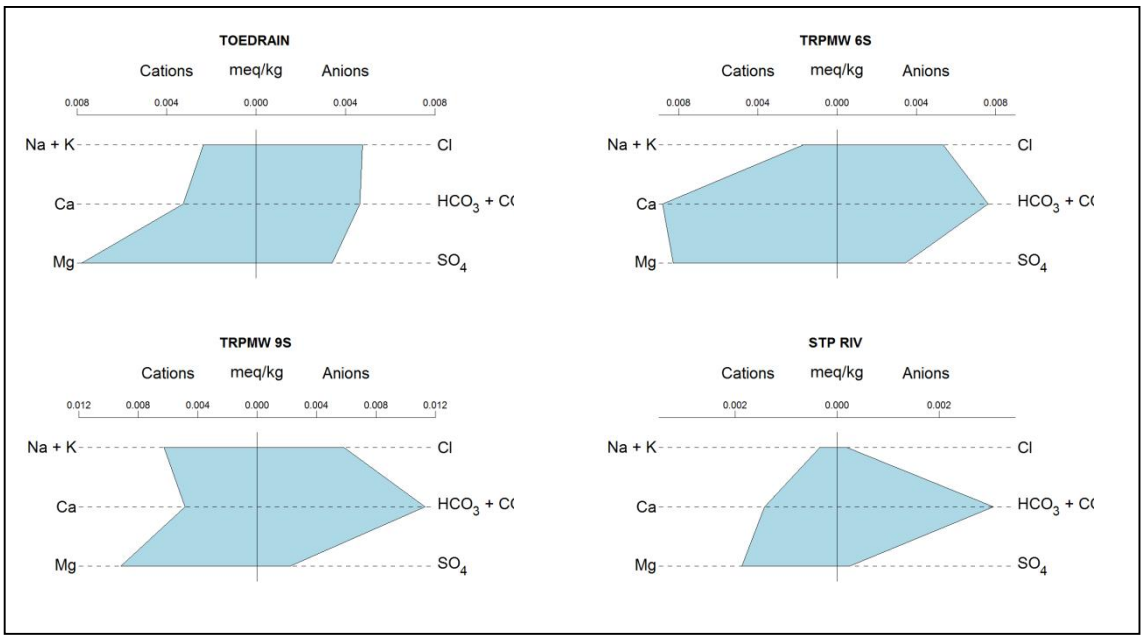

Figure 46: Stiff diagrams of major cations and anions in groundwater and surface water samples

Figure 47 also illustrates this possible link with a Piper diagram. The TOEDRAIN and TRPGWM6S samples plot in the quadrant representing Ca-SO_4 waters. This quadrant represents gypsum groundwaters and mine drainage. The TRPGWM9S and STP RIV samples plot in the quadrant representing Ca-HCO_3 waters. This quadrant represents shallow, fresh groundwaters. It should be noted that the TOEDRAIN and TRPGWM6S samples plot very close to the border line of the Ca-HCO_3 quadrant. This indicates that these samples have been only slightly influenced by mine drainage and if the SO_4 and Cl added from the tailings material were absent, these samples may also plot in the Ca-HCO_3 quadrant. This indicates that these samples may be linked by the same chemical fingerprint and contamination released from the tailings may reach the river. However, higher concentrations of major cations and anions were found in the groundwater as opposed to the river. This may be due to the dilution factor in the river. Therefore, the groundwater is believed to be the pathway in the system and groundwater users may be at higher risk of becoming potential receptors as opposed to river water users.

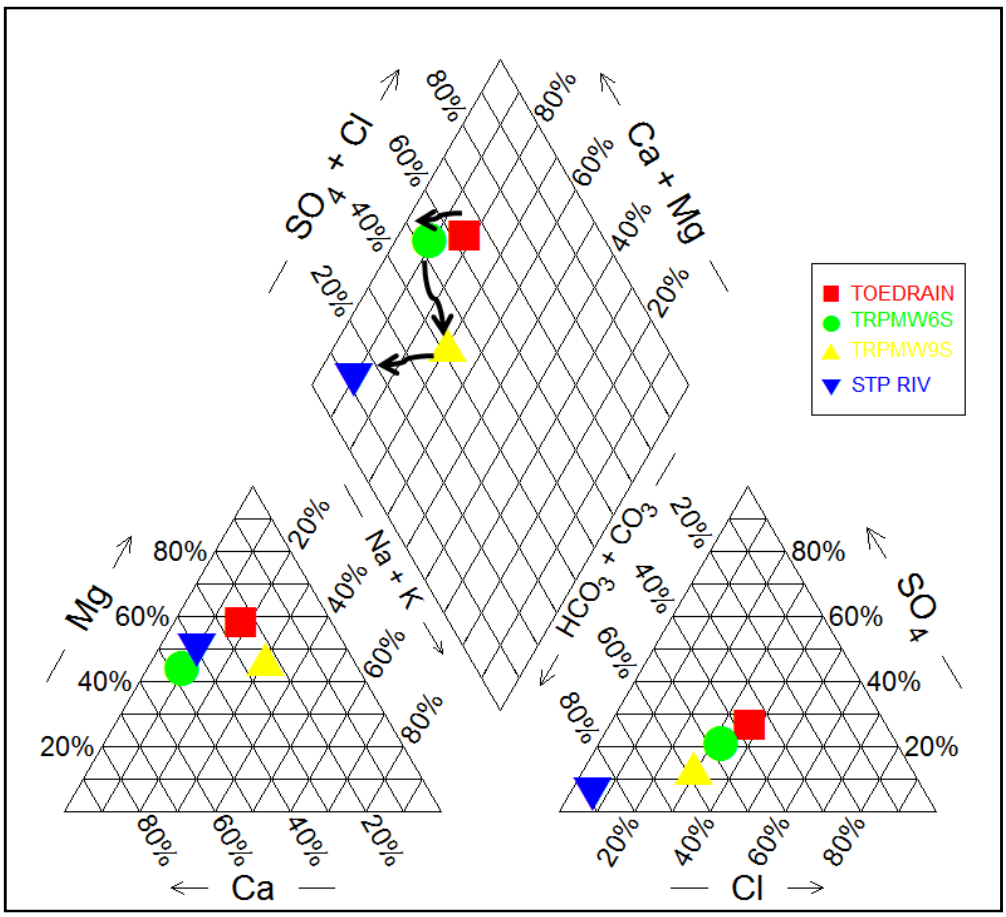

Figure 47: Piper diagram of groundwater sample chemical evolution

5.2 Hydraulic Testing

Hydraulic testing was performed on the tailings material as well as the underlying aquifer in the form of permeameter tests and pumping tests respectively. The values obtained from these tests were used to characterise fluid flow and groundwater flow velocities. The results of each test are described and discussed in the sections below.

5.2.1 Permeameter Tests

The values obtained from the falling head permeameter test are summarised below in Table 13. These values were interpreted to determine the saturated hydraulic conductivity of the tailings material. It is assumed that natural consolidation in the column will mimic field conditions in the TSF. Hydraulic conductivity for the tailings was calculated using the falling head permeameter equation in Craig (2004) and is denoted by the equation below:

$$K = 2.3\frac{al}{At_1}\log\frac{h_0}{h_1} \qquad \textit{Equation 6}$$

A hydraulic conductivity was calculated after each 30 minute interval of flow and an average value of 3.984 x 10^{-09} m.s^{-1} was obtained. This is in accordance with data published by Jorgensen *et al*. (1998) as well as Malmstrom *et al*. (2006).

Table 13: Summarised falling head permeameter test results

Time	Minutes	Seconds	Head (mm)	Drop (mm)	K (mm/s)
09:25	0.00	0.00	1530	0	
10:30	65.00	3900.00	1514	16	5.14568E-06
11:00	30.00	1800.00	1507	23	4.91478E-06
11:30	30.00	1800.00	1502	28	3.52455E-06
12:00	30.00	1800.00	1495	35	4.95413E-06
12:30	30.00	1800.00	1488	42	4.97738E-06
13:00	30.00	1800.00	1482	48	4.285E-06
13:30	30.00	1800.00	1477	53	3.58411E-06
14:00	30.00	1800.00	1471	59	4.31698E-06
14:30	30.00	1800.00	1466	64	3.61095E-06
15:00	30.00	1800.00	1461	69	3.62329E-06
15:30	30.00	1800.00	1456	74	3.63571E-06
16:00	30.00	1800.00	1451	79	3.64822E-06
16:30	30.00	1800.00	1448	82	2.19497E-06
17:00	30.00	1800.00	1444	86	2.93371E-06
17:30	30.00	1800.00	1438	92	4.41584E-06

This is indicative of a slow flow rate of water through the tailings material of an approximate order of magnitude of 10^{-4} m.d^{-1}. The amount of fluid that may discharge from the saturated tailings material (Q) was measured at approximately 0.34 L.d^{-1} through a cross sectional area of 1m^2, under a hydraulic gradient of approximately 1. However, the tailings material may not reach saturation throughout the profile under natural conditions. Therefore, the fluid discharged from the tailings may be less than 0.34 L.d^{-1} through the above mentioned cross sectional area and hydraulic gradient, as completely saturated flow does not necessarily occur throughout the tailings.

5.2.2 Pumping Tests – AQTESOLV

Two pumping tests were conducted on two monitoring wells adjacent to the TSF between 14 and 16 March 2012. The pumping test data was analysed to obtain hydraulic conductivity values for the underlying fractured aquifer using AQTESOLV software. The data obtained for TRPGWM06S is graphically illustrated below in *Figure 48*. The data obtained from this pumping test, conducted on the monitoring well closest to the tailings facility, was fitted with the Gringarten-Witherspoon curve assuming a single vertical fracture at depth. This method was chosen based on its provision of a hydraulic conductivity value for a fractured aquifer and provided a better fit than the Moench method. The underlying aquifer is also known to be fractured as it is composed of igneous rock, further supporting the use of this method. The curve provided by this method was fitted to the late time data to ensure that the hydraulic conductivity of the aquifer was calculated instead of the well bore storage. This yielded a K-value in the order of 0.46m/day for the underlying fracture network, assuming an anisotropy ratio of 0.5 between the horisontal and vertical axes.

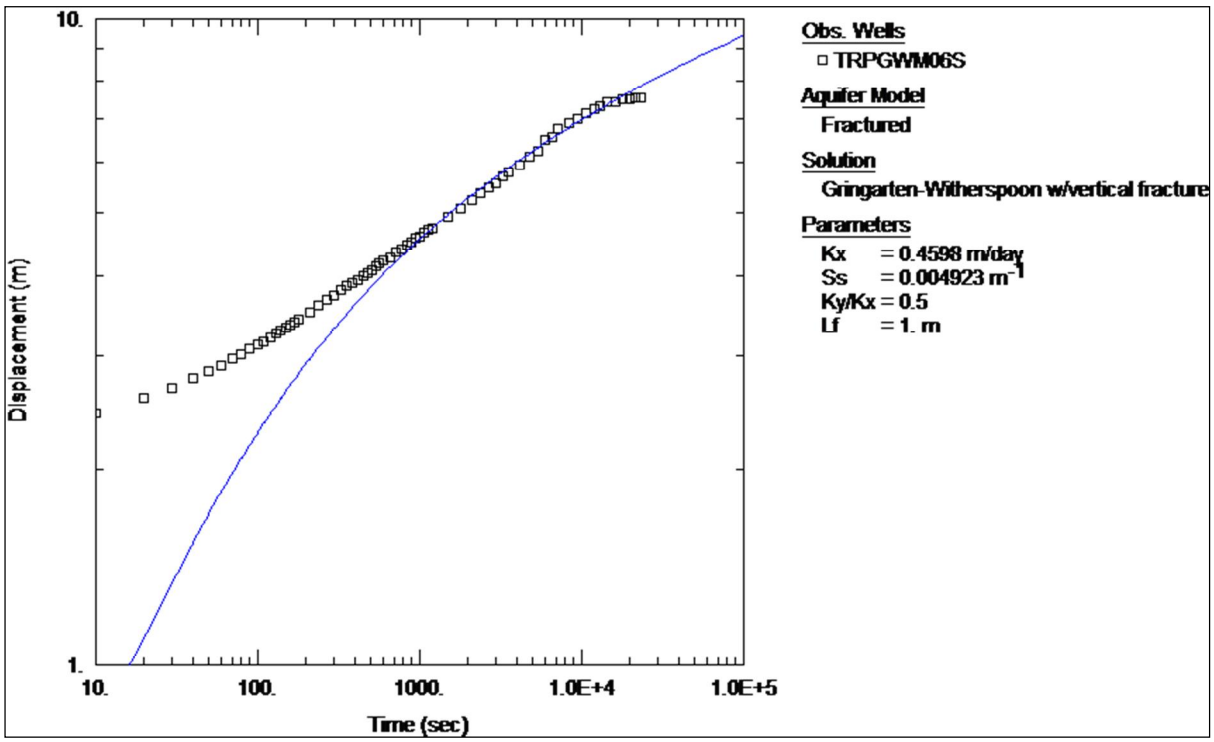

Figure 48: Pumping test data for TRPGWM06S fitted with Gringarten-Witherspoon on logarithmic axes

The linear flow velocity (equation below) in this portion of the aquifer was calculated as 0.015m/d of flow (Craig, 2004).

$$v = \frac{Ki}{\eta}$$ *Equation 7*

Where:

K: hydraulic conductivity
i: hydraulic gradient which is 0.0066 (calculated based on topography)
η: assumed porosity of 20% (comparatively low-conservative scenario)

This indicates a slow flow rate for groundwater in this portion of the aquifer and any accompanying contaminants may be transported at a rate equal to or slower than this rate. However, the properties of the aquifer will influence these flow and transport rate. This can be deduced from *Figure 49*. The flattening of the derivative curve around 10000 seconds and the abrupt dip in values that follows is indicative of a dual porosity aquifer. Therefore, components of a fractured and weathered aquifer system are both present in this portion of the aquifer and may influence the linear flow velocity of groundwater in different portions of the aquifer depending if the water moves through a more weathered, or more fractured portion.

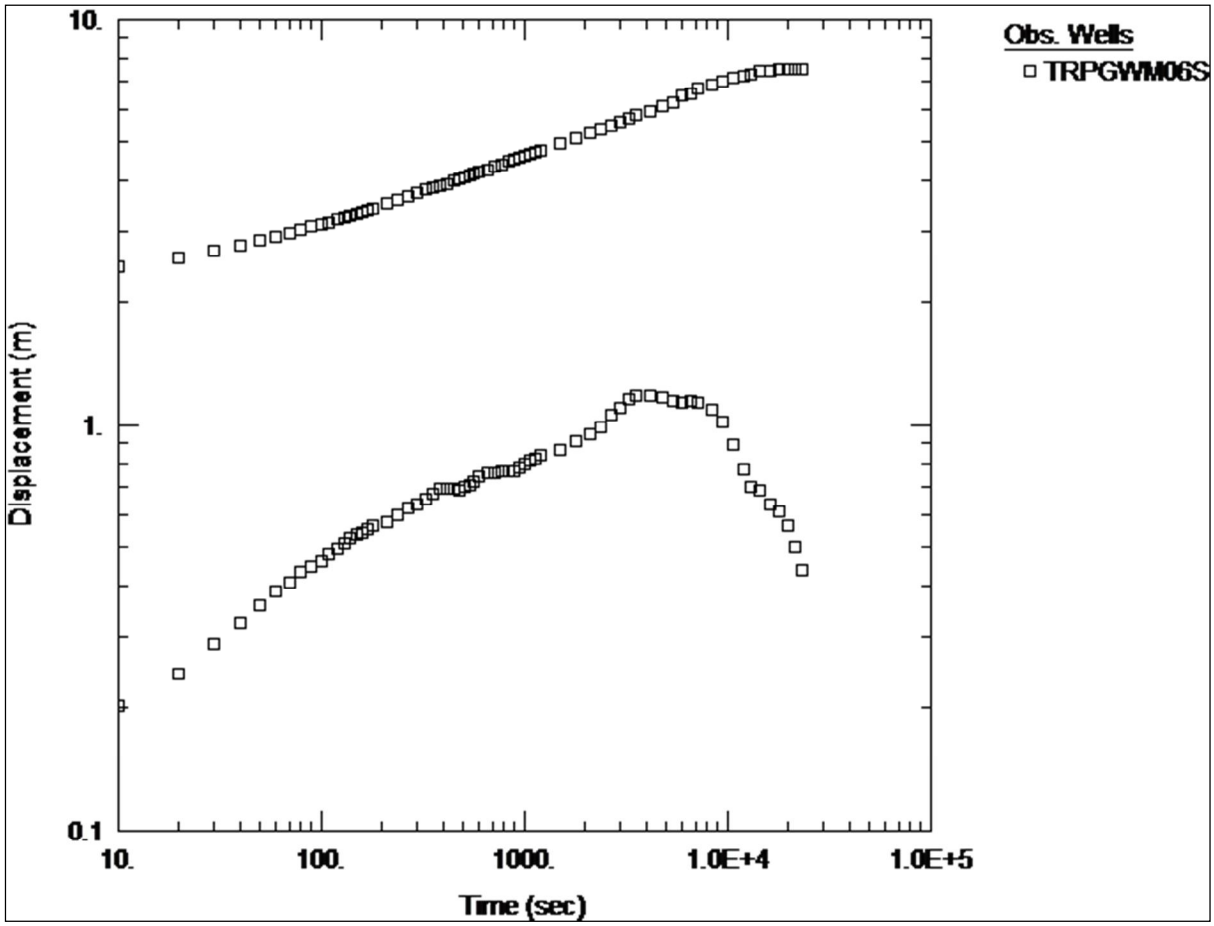

Figure 49: Derivative plot of TRPGWM06S

When comparing this information with that of TRPGWM09S, a slightly different situation is observed. This is indicated by *Figure 50*, which illustrates the pumping test data for the monitoring well TRPGWM09S. This well is situated closer to the Steelpoort river and further from the tailings facility. The data was also fitted with the Gringarten- Witherspoon curve for a single fracture, but provided a lower hydraulic conductivity in the order of 0.026m/day. The curve was also fitted to the late time data to ensure the representative calculation of the aquifer hydraulic conductivity, but used an anisotropy ratio of 0.1 between the vertical and horisontal axes. This improved the fit of the curve considerably but should be noted as an assumption. The linear flow velocity for this portion of the aquifer was calculated as 8.6×10^{-4} m/day, using the same assumptions for that of TRPGWM06S. This indicates a much slower rate of movement of groundwater than in the TRPGWM06S portion of the aquifer. It also indicates a much slower rate of contaminant advection due to groundwater stagnation and a higher salt load as indicated by *Figure 44* and *Figure 47*.

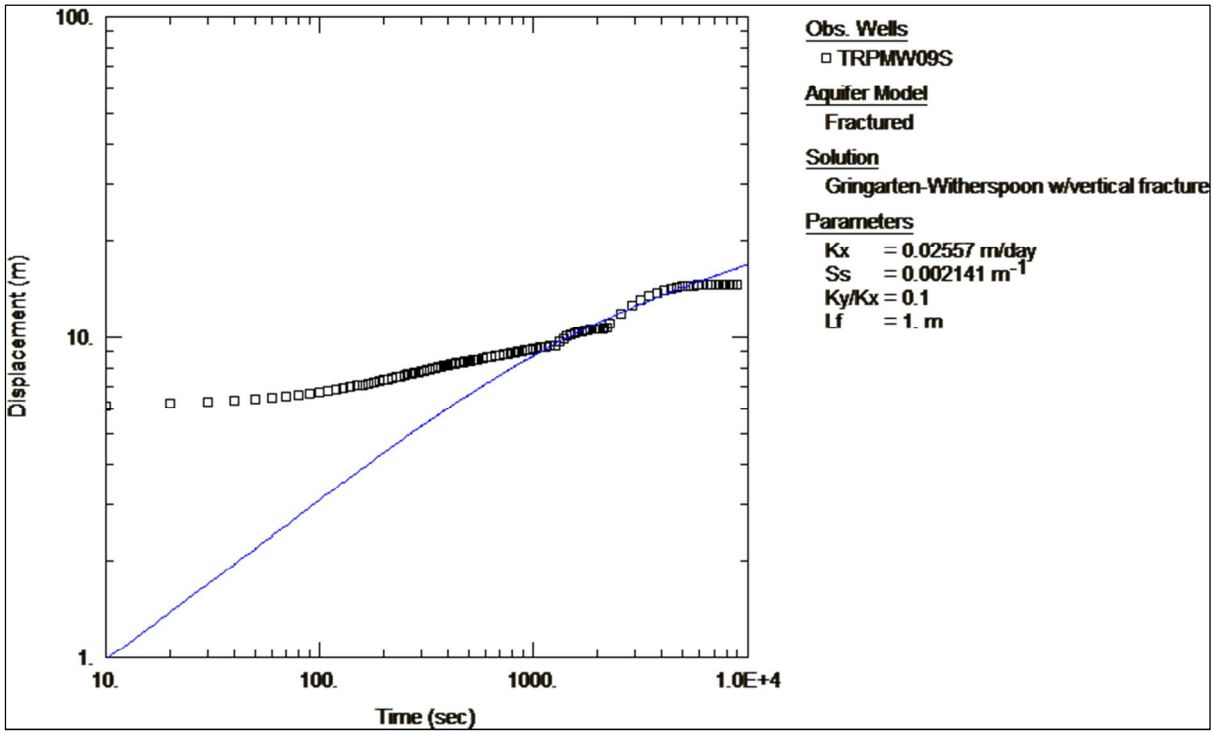

Figure 50: Pumping test data for TRPGWM09S fitted with Gringarten-Witherspoon

Another point to note in this figure is the doubling of the slope of the data at approximately 1000 and 2000 seconds. This change in the data's slope is possibly indicative of a low to no flow boundary encounter. The first doubling of the slope is believed to possibly indicate the Dwarsriver fault which is situated east of this monitoring well at a distance of approximately 550m. The second doubling of the slope may be a possible encounter of a second fault or could possibly indicate the encountering of the Steelpoort river. This may be supported by the levelling out of the data to provide a constant head reading around 10000 seconds with the waterlevel reaching 10.26m below groundlevel, close to the elevation of the river which is located at approximately 4m below the initial waterlevel in the borehole, measured at 5.95m. This may possibly indicate a hydraulic connection between the river and the aquifer, but more extensive pumping tests from more boreholes along the river are required to prove this conclusively.

Figure 51, the derivative plot of the data from TRPGWM09S, does however indicate that a fracture or fault structure was encountered between 1000 and 3000 seconds. The abrupt splitting of data and sharp slope change indicates a fracture or fault structure was encountered after which the water level became constant at around 4000 to 5000 seconds. The dip in derivative data between 300 and 1000 seconds indicates, similarly to that of TRPGWM06S, a dual porosity system. Therefore, components of a fractured and weathered aquifer system are also present in this portion of the aquifer at shallower depths and may influence the linear flow velocity of groundwater in different portions of the aquifer depending if the water moves through a more weathered, or more fractured portion.

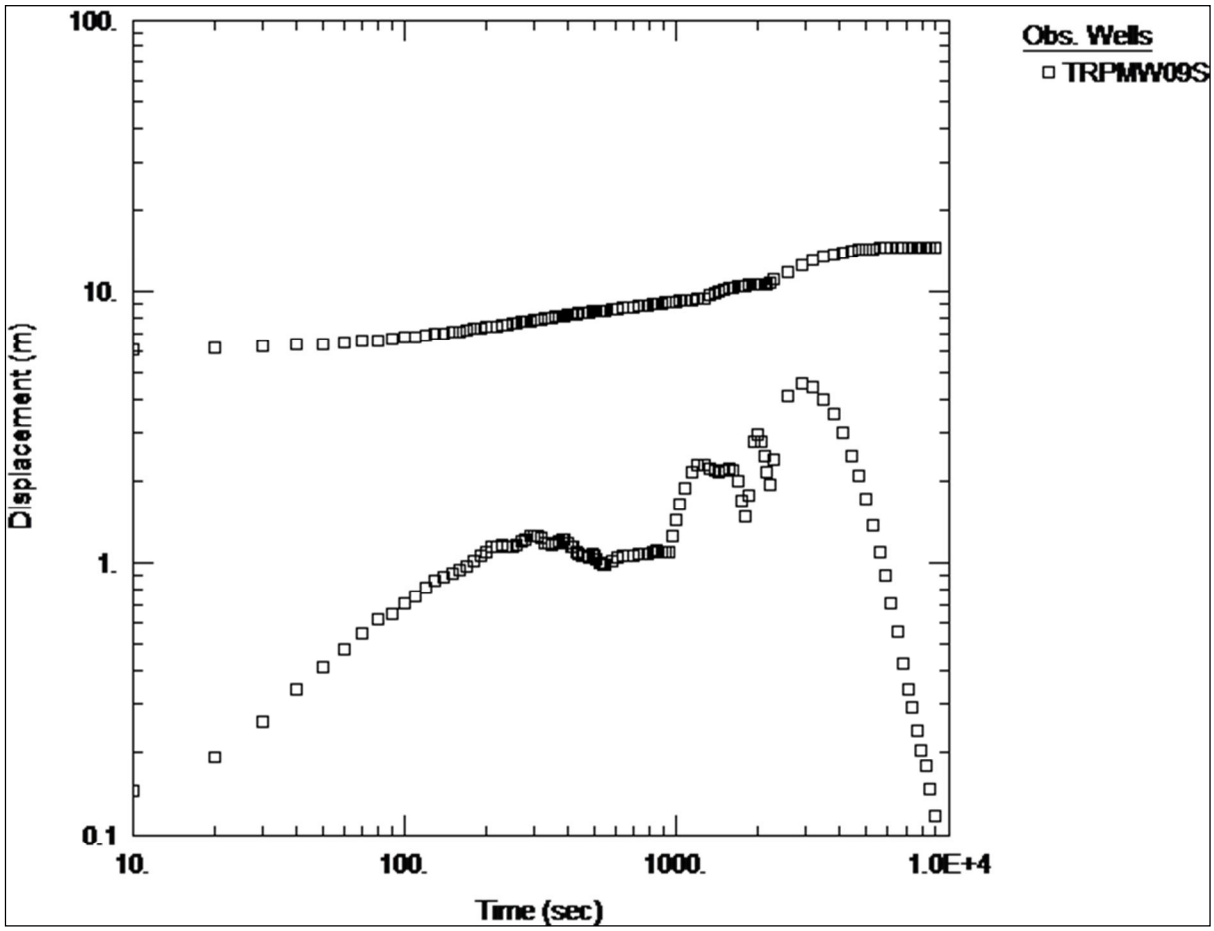

Figure 51: Derivative plot of TRPGWM09S

5.3 Geochemical and Unsaturated Flow Modelling

5.3.1 Geochemical Modelling – The Geochemist's Workbench

The modelling software used to determine the chemical changes taking place during fluid movement through the tailings-surface interface is The Geochemist's Workbench ©. The modelling software was used to calculate the breakdown of specific minerals, thought to be contributors to dissolved chemical components in groundwater and surface water, over a specified time period. This would give an indication of the geochemical processes taking place in the tailings causing contaminant release.

5.3.1.1 Model Construction and Assumptions

The model was constructed under the assumption that:

- Talc and chlorite are the phases most prone to breakdown as they are secondary in nature and may break down more rapidly than primary igneous minerals
- Chalcopyrite is considered to be prone to oxidise and dissolve readily in relation to primary igneous silicate minerals

- Oxygen fugacity from within the tailings to surface increases
- Oxygen fugacity from within the tailings to the aquifer decreases
- pH of the fluid in the tailings is slightly alkaline
- The leaching test values are a dilute representation of pore fluid within the tailings material
- Primary silicate phases as well as the chromite phase are practically insoluble in the scale of investigation based on literature values

The model was constructed using data from the acid leach tests, XRD analyses, ICP scans and literature, as follows:

- The acid leach test results were concentrated 20 times. The fluid to rock ratio in the leach test was noted as 20:1. Therefore, it was thought to be a reasonable assumption that the concentration of these values up to 20 times would give an indication of tailings pore fluid compositions as the leach test mobilises and dilutes pore fluids from a sample.
- The amount of fluid available for reaction was assumed to be an average of the measured gravimetric water content from the direct push probe samples for simplicity as the model would be a bulk composition simulation. This equated to 0.075kg of fluid per kg of rock material.
- The amounts of talc and chlorite present were taken as the average weight percentage throughout the tailings for simplicity as the model would be a bulk composition simulation. Rate constants were assigned to the phases as presented by Saldi *et al*. (2007) and Lowson *et al*. (2004) respectively.
- The amount of chalcopyrite present was taken as 0.01kg per kg of rock. This was assumed based on petrographic data as well as the acid-base accounting results. A rate constant was assigned to chalcopyrite as presented by Rimstidt *et al*. (1994)
- Oxygen fugacity was set to 2 orders of magnitude lower than the average atmospheric value of 0.21 to simulate a conservative case. The model was fitted with a sliding oxygen fugacity from 0.002 to atmospheric value to simulate discharge of the fluid from the tailings to the toedrain. A separate model was fitted with a sliding oxygen fugacity from 0.002 to 10^{-50} as a conservative case to simulate increasingly reducing conditions as tailings fluids discharge into the underlying fractured aquifer.
- After several model runs, a best fit of 60g of water addition upon discharge from the tailings was found to provide the best result, in terms of the short term calibration of the model to best provide long term calculations, and was therefore noted as an assumption.
- The concentrated leach test data was compared with the ICP analysis of the TOEDRAIN sample as well as the TRPGWM6S sample to determine the changes in fluid composition as illustrated in Figure 52. This data was used to calibrate the model to determine the neo-mineralised phases forming in and on the tailings, as well as the rate of mineral breakdown and contaminant input.
- The model was constructed to calculate geochemical changes within a 100 year period, to predict future concentrations of contaminants released from the material, with short term model runs only used for model calibration.

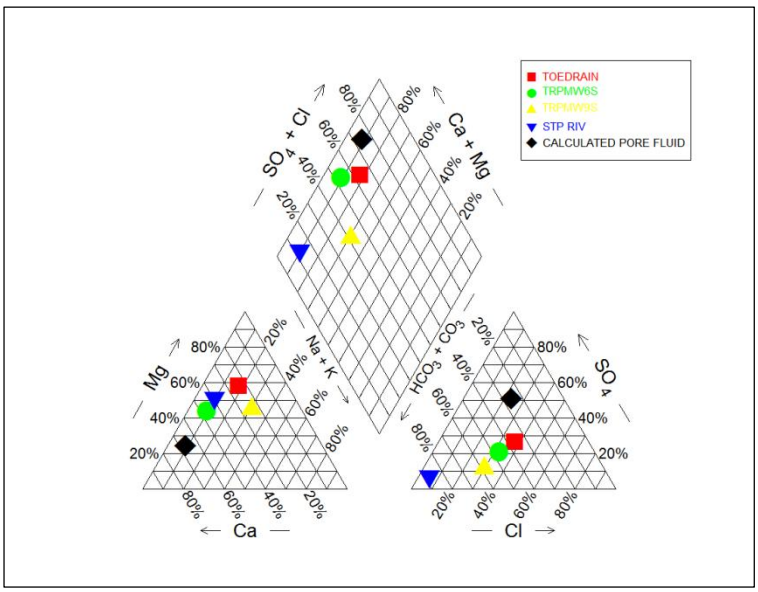

Figure 52: Piper diagram comparing groundwater, toedrain, river and tailings pore fluid compositions

5.3.1.2 Mineral Stability

The model constructed under the above mentioned assumptions calculated an immediate change in mineral abundances indicating breakdown as illustrated by *Figure 53*.

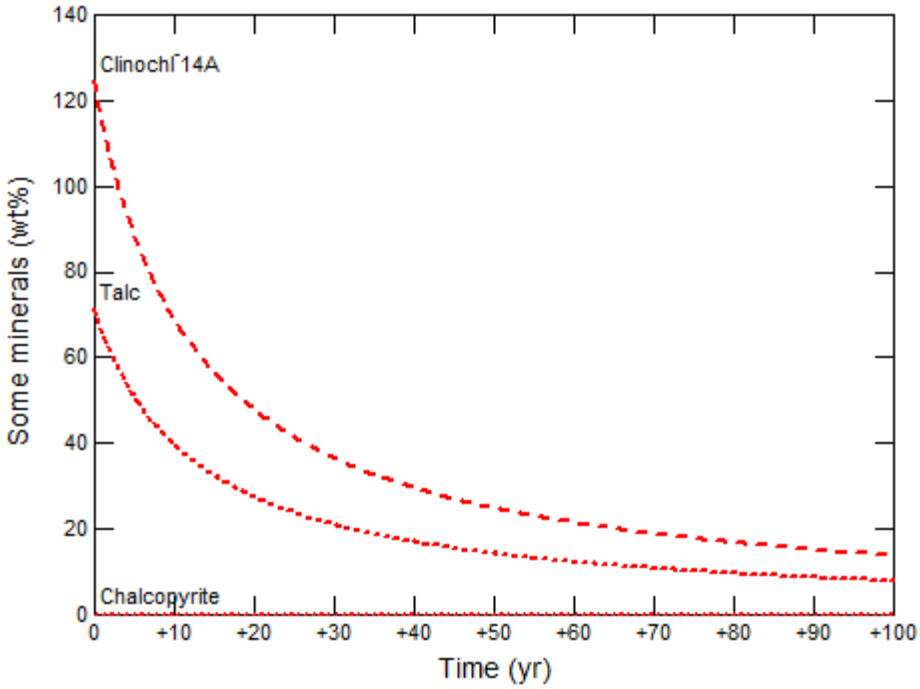

Figure 53: Modelled mineral phase breakdown

Figure 54: Precipitated salts and minerals on the tailings bank

This indicates that increased oxygen fugacity and fluid may accelerate mineral breakdown supporting the well known shrinking core model commonly used in tailings studies. Minerals exposed to atmospheric conditions and constant saturation may therefore produce more contaminants and salts as indicated by *Figure 54* which illustrates precipitated salts and discolouration on the saturated lower bank wall of the TSF.

According to the modelled data and factoring assumptions into account, talc, chalcopyrite and chlorite may be the major contributors to contamination in the short term. However, primary silicates and chromite may increase the contaminant load released from the material in the long term due to increased mineral breakdown and oxygen ingress.

The phases calculated by the model to form are illustrated below in *Figure 55* and *Figure 56*. The major phases calculated to form within the modelling period are gibbsite and a crystalline $CuFeO_2$ species. Gibbsite may possibly be derived from chlorite weathering and is precipitated from the solution as it has an alkaline pH value and no buffering Al is required to boost solution pH. This may also explain the low Al concentration in the analysed toedrain fluids. The $CuFeO_2$ phase, however, is considered less likely to form as intermediate salts are more likely to precipitate.

.

Goethite precipitation may also contribute to the lowering of the Fe-concentration in the toedrain sample and is also interpreted to be a possible precipitate of Fe in solution. Nontronite and beidellite are smectitic clay species which may form from the continuous alteration of chlorite and have a similar structure to this phase. However, talc may play a larger role in the formation of magnesian beidellite as this is a direct source of Mg. Calcic clinoptilolite is a low temperature zeolite and is interpreted to form at the base of the tailings where temperatures and pressures are elevated and may be a product of chlorite alteration.

The most likely phase to form from the permeating tailings pore fluid, which is also indicated by these figures, is predicted to be calcite. This phase may form due to the abundant Ca in the pore fluid solution and the possible change in CO_2 fugacity upon discharge from the tailings. This may also be substantiated by *Figure 54* which indicates precipitated salts on the tailings bank. Gypsum may also be a possible composition for these salts but is thought to be unlikely as the salts are only encountered on surface where a change in gas fugacity takes place which is not a driving force in the precipitation of gypsum.

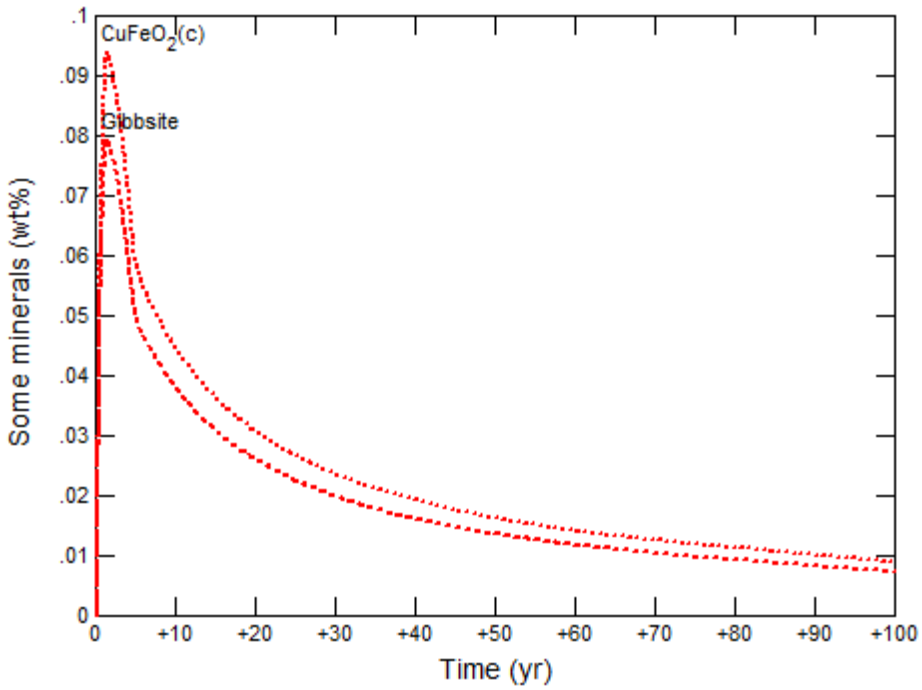

Figure 55: Model-calculated precipating major mineral phases

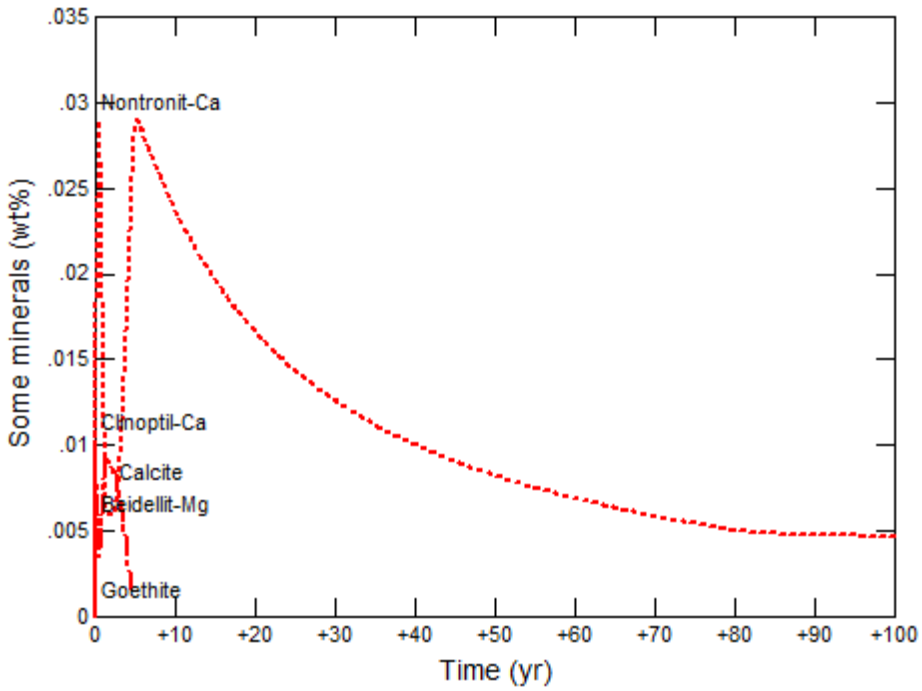

Figure 56: Model-calculated precipitated minor mineral phases

5.3.1.3 Liberated Contaminants

The modelled contaminants to be released from the tailings were a calibration of the model itself with respect to the pore fluid composition and the compositions of the TOEDRAIN and TRPGWM6S samples. However, it should be noted that these samples give a good indication of the composition of pore fluid discharge and contamination from the tailings and are therefore taken to represent the contaminant release from the material.

The modelled contaminant release is illustrated below in *Figure 57*.

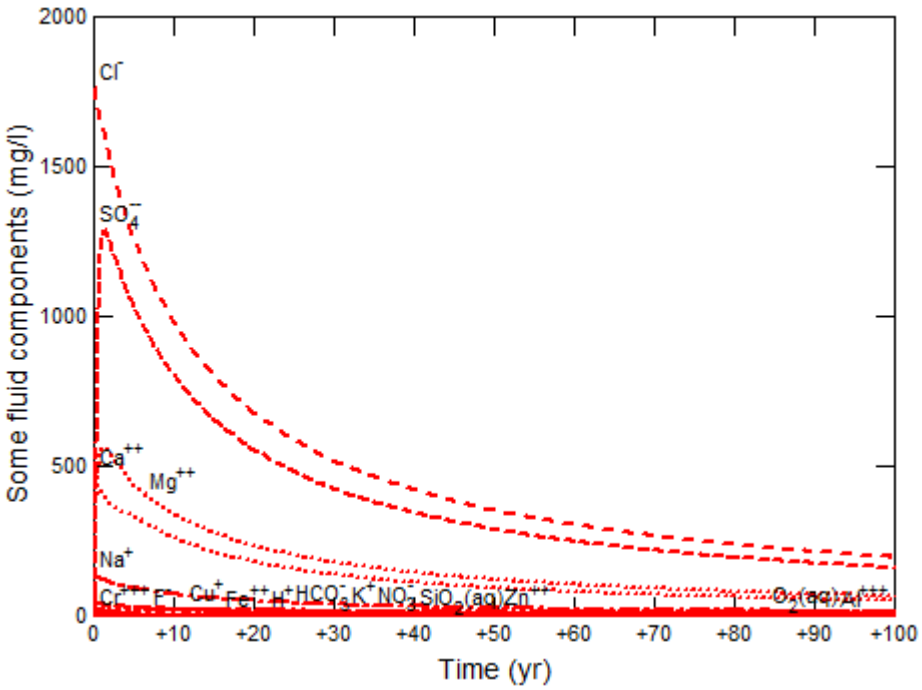

Figure 57: Modelled contaminant release from the tailings material as mg/L of constituents in contaminated water

This figure is of particular importance as it validates the model. The concentrations obtained from this model run were correlated with concentrations from the TOEDRAIN sample as well as the TRPGWM6S sample as illustrated in *Table 14* and *Figure 58*, as well as *Table **15*** and *Figure 59* respectively. Each data point was fitted with a standard error to determine if the sample concentrations and model concentrations correlate well within statistical error boundaries. The modelled concentrations were found to correspond well with the analytical values and the results obtained for mineral phase precipitation, formation and breakdown are therefore thought to be valid.

Table 14: Modelled and analysed concentrations of chemical constituents in TOEDRAIN sample

Constituent	Model (mg/L)	Analysed (mg/L)
Ca	52.49	66
Mg	76.28	96
SO_4	161	165
Cl	195.7	171
Al	0.05	0.156
Cr	0.04	0.025>
K	4.3	1.7
Si	2.7	9.5
NO_3	3.7	1.6

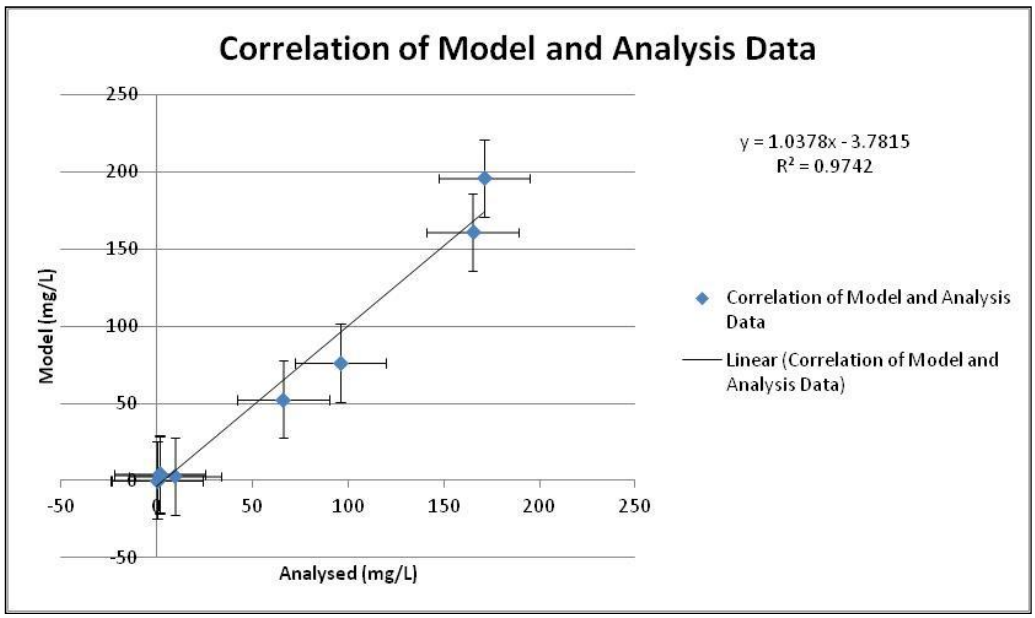

Figure 58: Correlation of modelled and analysed concentrations of chemical constituents in TOEDRAIN sample

Table 15: Modelled and analysed concentrations of chemical constituents in TRPGWM6S sample

Constituent	Model (mg/L)	Analysed (mg/L)
Ca	69.15	179
Mg	53.02	102
SO4	161.6	168
Cl	195.2	192
Al	0.02	0.177
Cr	0.04	0.025>
K	4.3	1.0>
Si	1.168	14.6
NO3	4.73	11

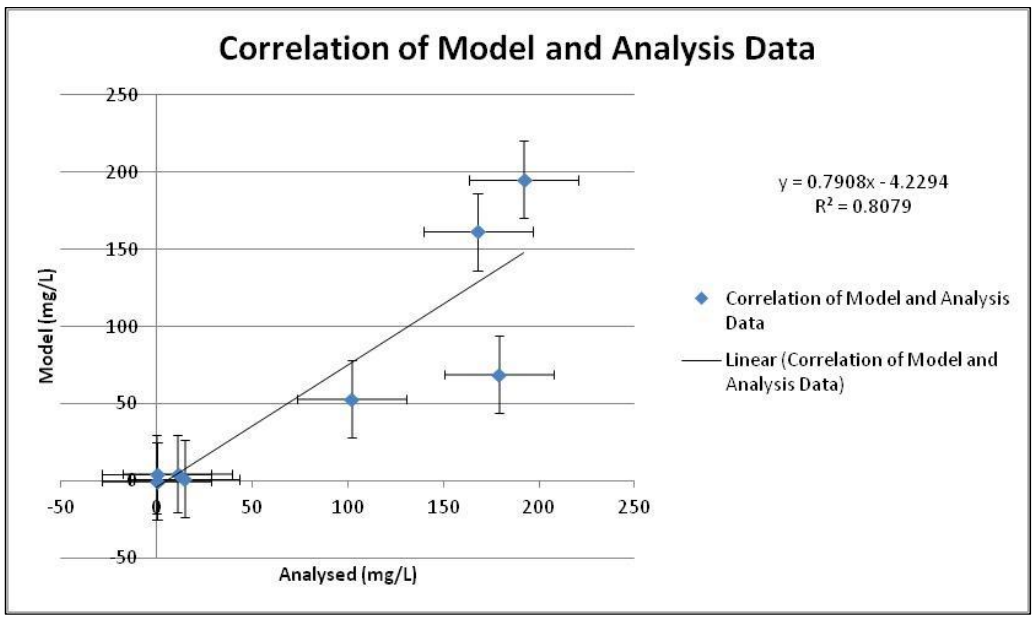

Figure 59: Correlation of modelled and analysed concentrations of chemical constituents in TOEDRAIN sample

5.3.2 Unsaturated Flow Modelling – HYDRUS

The modelling software used to determine the unsaturated hydraulic properties of the tailings material is HYDRUS1D 4. The model was used to calculate cumulative rainfall infiltration over a ten year period; change in water content over a period of ten years considering past meteorological data; water content at specified observation nodes in the profile over a ten year period; hydraulic conductivity of the material and underlying vadose zone at different degrees of saturation; and fluid flux from the bottom of the tailings. The modelled values are graphically illustrated and discussed in the following section.

5.3.2.1 Model Construction

The model was constructed using data measured from the direct push probe samples obtained from the TPH sampling point. Gravimetric water contents were measured from each sample tube and are summarised in *Table 16*.

Table 16: Measured gravimetric water contents from the TPH sampling locality

Sample Depth	Material Type	Initial Mass	Dry Mass	ΔMass	Gravimetric Water Content
0-1.2	Tailings	21	20.5	0.5	2.380952381
1.2-2.4	Tailings	17	16	1	5.882352941
2.4-3.6	Tailings	22	20	2	9.090909091
3.6-4.8	Tailings	31	30	1	3.225806452
4.8-6	Tailings	32	30	2	6.25
6-7.2	Tailings	38	34	4	10.52631579
7.2-8.4	Tailings	26	24	2	7.692307692
8.4-9.6	Tailings	29	24	5	17.24137931
9.6-10	Gravelly Sand	17	16	1	5.882352941

The tailings material is known to be of a -86µm grading and was therefore classified as a silty clay in soil terms. The underlying soil in the natural vadose zone was found to be a coarse gravelly sand.

Once these parameters were ascertained, the unsaturated flow model was constructed as follows:

- The sole simulation to be performed by the model was specified as water flow. Heat-, vapour- and CO_2 transport was not a modelling objective and was therefore omitted.
- Two sediment materials were specified, each representing the tailings and underlying soil. The combined depth of the materials in the profile was specified as 10m with measurement units specified as meters.
- Time units were specified as years with a starting time of 0 and an ending time of 10. Default values were used for maximum-, minimum- and initial time step. Ten years was chosen as the model simulation time based on the saturated hydraulic conductivity calculated from the falling head permeameter testing. Theoretically, under saturated conditions, this would be the time frame for contaminated fluid to move from the top, to the base of the tailings.
- The number of time variable boundary conditions was specified as ten. These conditions represent rainfall data.
- Default values were used for the printing information section as well as in the iteration criteria section. However, in iteration criteria section, water content tolerance was specified as 0.0001 to allow the model to run to a value near desiccation if required.

- The mobile-immobile dual porosity hydraulic model with water content and mass transfer was used to simulate flow as two sediment materials exist in the profile.
- The sediment hydraulic parameters were chosen based on the sediment characteristics such grading, bulk density and saturated hydraulic conductivity. This was performed using the neural network prediction function of HYDRUS.
- The upper boundary condition of the profile was specified as Atmospheric BC with surface runoff with a free draining lower boundary condition as the underlying soil material is coarser than the tailings material. The initial condition of the system in terms of fluids was specified in water contents.
- The graphical discretisation tool of HYDRUS was used to discretise the water content- and material distribution of the profile as well as to specify model observation nodes at 1m intervals in the profile.

5.3.2.2 Model Execution and Results

After model construction was completed, the model was executed and the following parameters were calculated and interpreted with respect to the tailings storage facility. The model was constructed to illustrate a conservative scenario which assumes complete infiltration of rainfall.

Cumulative Rainfall Infiltration

Assuming a completely unsaturated top of the tailings material, the infiltration of rainfall would take place rapidly and infiltrate into deeper levels in the TSF profile. This is directly linked to the amount of rainfall in a particular year of the simulation. The time dependent boundary condition linked to rainfall in the simulation, was based on the mean annual precipitation of the area since 2001. Therefore, a curve can be observed indicating similar trends to rainfall per year. Evaporative losses were omitted from the calculation to create a conservative scenario indicating the maximum amount of fluid recharged into the tailings. Based on these assumptions, the model calculated a maximum cumulative rainfall infiltration of approximately 3500mm per decade. This is illustrated in *Figure 60*.

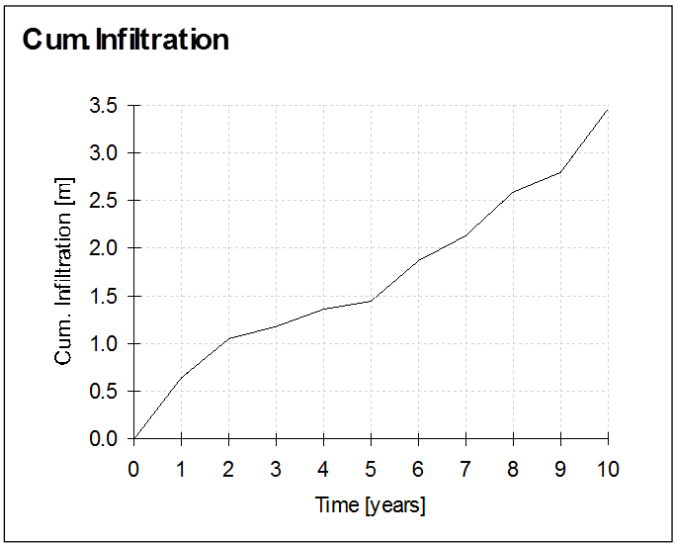

Figure 60: Cumulative rainfall infiltration per decade for the tailings material

Change in Water Content Considering Past Meteorological Data

Initial soil moisture content was specified at different depths in the soil profile as mentioned in the model construction section. However, when simulating rainfall events in the model, these moisture contents vary due to the infiltration of rainwater and percolation through the profile. This variation is illustrated by *Figure 61*, where water content is illustrated with depth for each year of the simulation. Each year is indicated by a different colour and T-value in the legend. As illustrated, the void space, which was assumed to be between 20 and 30% for the tailings material grading by the model, becomes completely filled with fluid after the ten year duration of the model simulation. The coarser underlying soil material also becomes saturated after 7 years in the simulation. This could be explained by the smaller porosity of the coarser material allowing for less fluid to saturate the material.

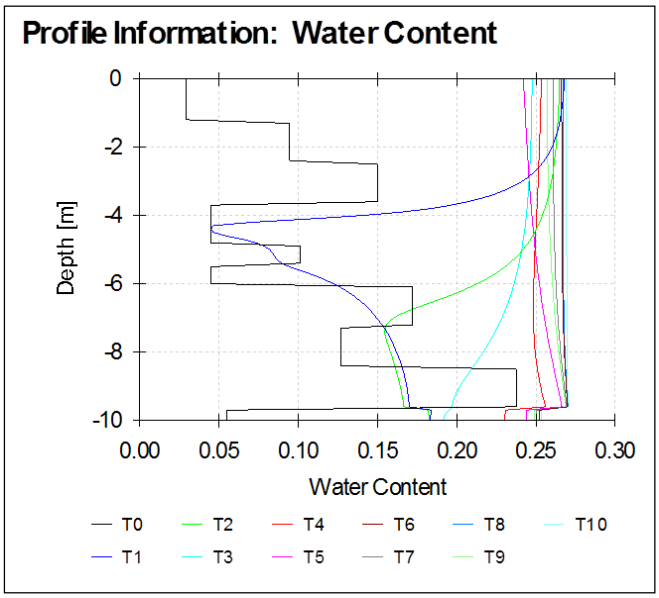

Figure 61: Tailings water content at different depths and times

The possible reason for the saturation of the material will be explained in the following sections. Another important simulation pertaining to the material water content, as generated by the model, is graphically illustrated in *Figure 62*. This figure illustrates the water contents present at each specified observation node in the profile with time. Each node number is denoted by the prefix N. It can be observed that the curve for each node moves sequentially forward relative to the time axis in a chronological order while the curve also indicates an increase and decrease in water content with time with a similar trend to that of annual rainfall. The sequential shifting of each curve may possibly indicate a piston flow regime with water movement taking place due to a change in pressure head by infiltration. The data can also be observed to contain an inverse logarithmic trend indicating faster infiltration at the top of the profile and slower infiltration lower in the profile due to higher degrees of saturation. Node ten can also be observed to have an anomalous curve which indicates the saturation of the underlying soil material at a lower water content and is illustrated well relative to node 9 which is located at the bottom of the tailings material. Node nine also shows an anomalously high final water content. This is due to ponding of fluids at the boundary between the coarser and finer sediments due to higher suction values in the tailings material.

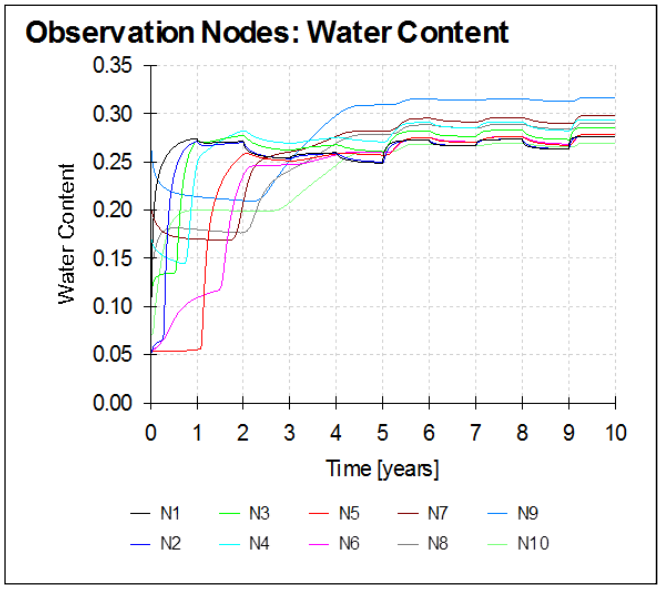

Figure 62: Water content at profile observation nodes at different simulation times

Cumulative Bottom Flux

The cumulative fluid flux from the bottom of the tailings is a function of the cumulative infiltration and the change in fluid content stored pore as pore water in the tailings. This parameter is important to quantify the possible amount of leachate released from the tailings into the vadose zone and possibly the groundwater. Assuming complete infiltration of rainfall as well as the possibility of changes in pore fluid content, the model calculated an average cumulative discharge of 1.9m per decade, from the base of the tailings, as indicated by *Figure 63*. This indicates approximately 0.19m of discharge per year through a cross-sectional area of $1m^2$. Therefore, approximately $190L/m^2/y$ of leachate is released through the foot of the tailings as a conservative scenario, completely discounting lateral fluid discharge. However, as it is known that tailings water is released through the tailings wall into toedrains, the volume of leachate released into the groundwater environment is expected to be significantly less.

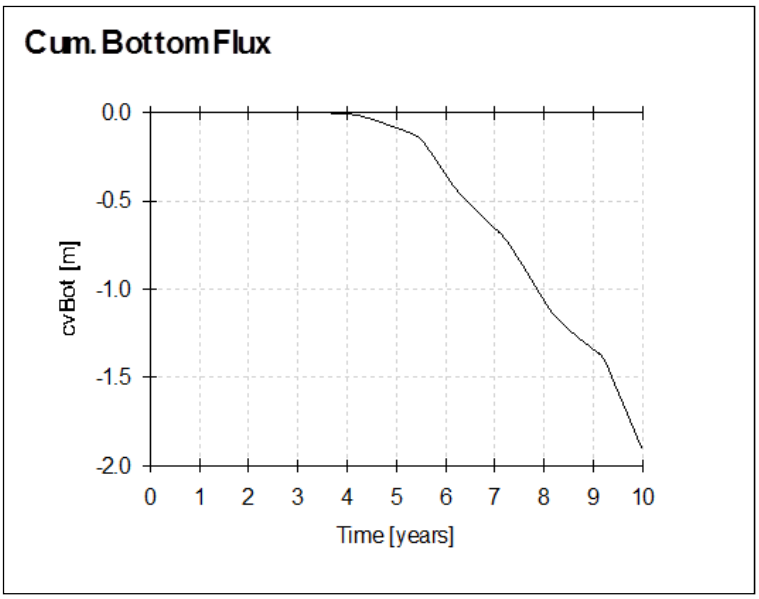

Figure 63: Cumulative fluid flux from the foot of the tailings as a conservative case

Unsaturated Hydraulic Conductivity

The saturated hydraulic conductivity was measured to be approximately 1.2m/decade ($3.29x10^{-4}$m/d). Based on the textural class and moisture contents of the tailings profile and assuming a porosity of 25%, the model predicted a hydraulic conductivity value in the same order of magnitude, for the saturated tailings profile. The model was therefore assumed to be acceptably representative based on its agreement with experimental data. The model also calculated unsaturated hydraulic conductivities for the tailings material and based on the varying degrees of saturation from the top to the bottom of the tailings, water could be conducted through the material at rates of between 10^{-8} m/decade and 1m/decade. These values were calculated between water contents of approximately 5 and 27% respectively. This is illustrated by *Figure 64* in which M1 represents the tailings material.

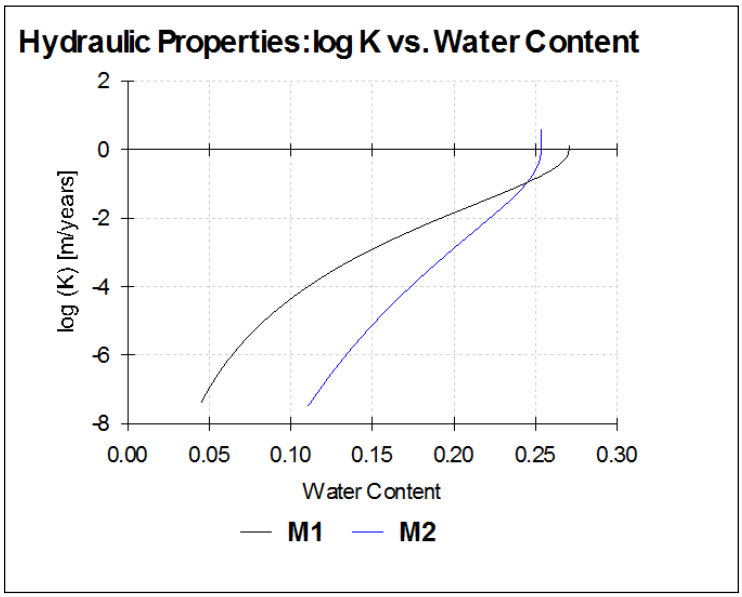

Figure 64: Unsaturated hydraulic conductivities at different water contents in the tailings material (M1) and the underlying, natural gravelly sand vadose zone (M2)

M2 in *Figure 64* illustrates the underlying gravelly sand of the natural vadose zone. Water is predicted to move at faster rates at higher degrees of saturation and slower rates at lower degrees of saturation in this material. The natural vadose zone is therefore less conductive than the tailings at most pore water content values below approximately 24% which may explain the fluid ponding in the lower areas of the tailings profile. The unsaturated hydraulic conductivity of the underlying vadose zone was calculated to range between 10^{-8} m/decade and $10^{0.5}$m/decade. These values were calculated for water contents ranging approximately between 11 and 26% respectively.

6. CONCLUSIONS

Based on the data collected; analyses and tests performed; assumptions and interpretations made; and models calculated, the following conclusions could be made:

1. The chemical composition of the tailings material is dominated by the major elements Mg, Ca, Fe, Si, Al and Cr based on XRF results. The dominant trace elements contributing to the tailings material composition are Sc, Ni, Zn and Co.
2. The mineralogical composition of the tailings material consists of the following:
    - Annite $KFe_3(Al, Si)_3O_{10}(OH, F)_2$
    - Anthophyllite $(Mg_{0.76}, Fe_{1.24})(Mg_{4.95}, Fe_{0.05})Si_8O_{22}(OH)_2$
    - Diopside $(Ca, Mg)Si_2O_6$
    - Enstatite $(Mg_{1.568}, Fe_{0.432})Si_2O_6$
    - Magnesiohornblende $Na_{0.46}Ca_{1.7}Mg_{3.44}Fe_{1.72}Al_{1.08}Si_{6.92}O_{23}(OH)$
    - Lizardite $Mg_3Si_2O_5(OH)_4$
    - Chromite $NiCr_2O_4$
    - Anorthite $CaAl_2Si_2O_8$
    - Talc $Mg_3Si_4O_{10}(OH)_2$
    - Chlorite (Clinochlore) $Mg_{5.1}Al_{1.2}Si_3Cr_{0.7}O_{10}(OH)_8$
    - Phlogopite $KMg_3(Al, Si)_3O_{10}(OH,F)_2$
    - Muscovite $KAl_3Si_3O_{10}(OH)_2$
    - Tremolite $Ca_2Mg_5Si_8O_{22}(OH)_2$
    - Chalcopyrite $CuFeS_2$
3. The dissolution potential of the mineral phases is considered to be low even under oxidising, saturated conditions as the alkaline fluid draining through the tailings material favours slightly lower reaction rate constants. This causes primary minerals to break down in a geological time scale, superseding the scale of investigation as well as the life of mine. However, alteration phases such as talc and chlorite as well as the sulphide phase, chalcopyrite, are likely to break down in the scale of investigation. This may form precipitated salts, clay minerals and possible low temperature zeolites at the interface between the tailings and earth surface conditions.
4. The major contaminants released by the tailings material are Ca, Mg, SO_4 and Cl which may increase groundwater salinity, but due to groundwater alkalinity, the probability of acid rock drainage formation is low. Trace heavy metal contamination is considered unlikely as these elements were either undetected or detected in low concentrations in toedrain fluids. These trace metals are mainly associated with the chromite phase which is considered practically insoluble in the tailings redox conditions. Chromite is considered to break down in reducing, acidic conditions, both of which were not found to be present in the tailings storage facility.
5. The fluid discharge from the tailings was identified as 2m per decade with ingress of 3m per decade from rain water. The hydraulic conductivity of the tailings material was found to range between 10^{-8} and 1m/decade. These values were calculated between water contents of approximately 5 and 27% respectively. The unsaturated hydraulic conductivity of the underlying vadose zone was calculated to range between 10^{-8} and $10^{0.5}$m/decade. These values were calculated for water contents ranging approximately between 11 and 26% respectively. Fluid and contaminant movement through the tailings material is considered as porous medium flow.

6. The hydraulic conductivity of the aquifer was found to be 0.46m/d in the area of the aquifer underlying the tailings. The hydraulic conductivity of the aquifer was found to be 0.026m/d in the area of the aquifer closer to the Steelpoort river. Two no flow boundaries were encountered during the pumping tests which were interpreted as part of the Dwarsriver fault system. The second derivative of the pumping test curves indicated that the aquifer is a dual-porosity system. However, water and contaminant movement is considered predominantly as fracture flow.

The interconnection between the fractured rock aquifer underlying the tailings storage facility and the tailings material is evident in the water chemistry analysed. A contaminant load is imposed on the aquifer by permeating fluids. This contaminant load is generated by geochemical processes causing mineral breakdown in the tailings material. However, no acid rock drainage is likely to form and no significant heavy metal contamination is likely to take place. Based on the study, only groundwater salinity will be elevated by discharge of the chemical constituents released by geochemical processes from the tailings material. The Steelpoort river also shows a different chemical signature than the groundwater and tailings fluids which; along with the increase in chemical concentrations in the groundwater closer to the river, indicating stagnation and evaporation; as well as no flow boundaries indicated by pumping tests; indicates that the river may not be significantly impacted by chemical discharge from the tailings.